INVESTIGATION AT LOW SPEED OF A SIX-PERCENT THICK SYMMETRICAL CIRCULAR-ARC AIRFOIL WITH LEADING EDGE RETRACTION IN COMBINATION WITH NOSE SLOT

Thesis by

Carl Birdwell, Jr.

Lieutenant, United States Navy

In Partial Fulfillment of the Requirements

for the Degree of

Aeronautical Engineer

California Institute of Technology

Pasadena, California

1955

ACKNOWLEDGMENTS

The author is indebted to Dr. H. J. Stewart and Dr. Anatol Roshko, of the GALCIT staff, for valuable advice and guidance.

The author also wishes to recognize his colleague and collaborator in the investigation, Lt. Robert F. Doss, USN, who originated the idea and has written a separate thesis using the same data.

SUMMARY

The effectiveness of leading-edge retraction as a possible high-lift device for thin, sharp-nosed airfoils was investigated. Experimental results are presented for a symmetrical, 6%-thick, circular-arc airfoil configuration, such that the forward 9.5% section of the chord is retractable up to a distance of 20% chord into the wing. The results include direct force measurements, limited surface pressure surveys and limited single-tuft surveys.

Tests were made with varying amounts of retraction in combination with variable stagger between leading edges of upper and lower surfaces and with several upper surface slot configurations. One retracted configuration was tested with a 20% chord, split-flap.

The results show that retraction is ineffective in increasing maximum lift. In general the effect on maximum lift was as follows: (1) Retracting up to approximately 9%, decreased maximum lift in proportion to the loss in wing area, (2) With exactly 9.06% retraction and with certain configurations of stagger and/or slots, the stalling angle of attack was increased 2° and the maximum lift was equal to that of the unaltered airfoil, (3) Retracting more than 9.06% resulted in a disproportionate loss of maximum lift, approximately 20% less than the unaltered airfoil.

TABLE OF CONTENTS

I. INTRODUCTION

For sustained flight well into the supersonic regime it has been established that a very thin wing with sharp leading edges is a practical necessity. Although possessing reasonable aerodynamic properties at high speeds, these thin wings perform poorly at low speeds. Due to early flow separation near the leading edge, the maximum lift coefficient of the sharp-nosed airfoil is considerably reduced in comparison to a typical subsonic section.

Two important problems arise that are associated with low maximum lift coefficient as applied to a supersonic airplane with high wing loading:

(1) Higher take-off and landing speeds. The attendant evils of this problem are many and varied. Of prime concern are safety and the excessive length of runway required for unassisted take-off or non-arrested landing. The problem becomes acute on aircraft carriers where higher landing speed demands more exacting pilot technique and arresting gear of larger capacity to absorb the substantially greater kinetic energy.

(2) Loss in high altitude maneuvering ability. The combined effect of low maximum lift coefficient and low density is to restrict the acceleration that may be imposed on the aircraft during a turning or pull-up maneuver without stalling.

These problems have led to many investigations of high lift devices applied to the circular-arc and double-wedge airfoils. References 1 to 8 are representative. Trailing edge flaps, leading edge flaps, slots,

slats, area suction, ejection of air tangential to the wing surface and various combinations thereof have been shown to be effective. Because all of these devices present serious structural problems when applied to extremely thin wings, say four percent thick, it was felt desirable to investigate the effectiveness of a somewhat simpler device, namely that of retracting a small portion of the sharp leading edge.

Experimental investigations into the details of the flow about thin, sharp-nosed airfoils (Ref. 9) have shown that laminar separation occurs almost immediately upon increasing the angle of attack from zero. While separated, transition to turbulent flow apparently occurs and the boundary layer reattaches at some point downstream depending on the angle of attack. The limiting case where the flow reattachment is coincident with the trailing edge determines the stall and in this condition the laminar separation "bubble" extends over the entire chord. (This type of stall is distinctively different from the abrupt, leading-edge separation which characterises the stall of medium thick, blunt-nosed airfoils.) The mechanics of reattachment has not been fully explained in the presently available literature, but it appears reasonable that the initial separation near the nose is due to the shift of the stagnation point to the lower surface with angle of attack. The flow, in passing from the stagnation point around the leading edge, is unable to attain the theoretical infinite velocity (for infinitely sharp leading edges) and takes the "path of least resistance", which apparently is to separate.

On this basis it seemed likely that some control over the location of the stagnation point might be effected by retracting a portion of the sharp leading-edge into the wing. The overall leading edge after retraction would consist of three separate edges spaced slightly apart. The leading

edge radius would effectively be increased and an increase in maximum lift should result (Ref. 7). The resulting gap between the upper and lower surfaces after retraction provides an inlet and a internal channel which could be used advantageously with a slot opening to the upper surface. With the existence of a favorable pressure differential, this slot should partially re-energize the boundary layer resulting in a further improvement of the flow.

The manifest effect of this scheme is a certain loss in lift due to a decrease in wing area. Therefore, to be of practical importance, the device must produce an increment of lift over and above the loss due to reduction in area.

II. DESCRIPTION OF MODEL AND TESTS

The basic model used in all of these tests was a symmetrical circular-arc airfoil with a rectangular planform. The circular-arc profile was selected because it is thicker near the nose (cf. double-wedge), thus allowing more space, at a given chordwise station, to form the retracting part. The model was constructed in segments (see Figs. 1 and 2) in order to form the several sectional configurations and to allow retraction of the nose piece. The basic dimensions are: span - 24", chord - 10", thickness - 6%, radius defining the contour - 41.817". The several parts were machined from solid brass and hand-worked to a smooth finish. The after 50% of the chord served as a base to which the forward pieces were attached. These pieces were fastened with counter-bored machine screws and the counter-holes filled with wind tunnel wax.

The slot was formed by sawing the top piece into two parts along a line where the slot was to be located. The leading edge of the aft part was built-up with solder and machined to contour. The fore part was machined to shape and re-mounted using a number of chordwise struts. (See Figs. 4 and 5a)

Circular endplates, 15" in diameter, were used to approximate two-dimensional flow conditions. These plates were cut from 0.125" thick, 24ST aluminum alloy and the edges machined to a 15° bevel to minimize the boundary layer on the sides toward the model.

The leading edge piece extended laterally into longitudinal slots milled into the end plates and was secured with machine screws passing through the plates in slightly narrower slots. The slots were of sufficient length to permit fore and aft movement of the leading-edge piece to any desired re-

traction up to 20% of the chord.

The model was supported upright in the wind tunnel by a three-point suspension system. Two streamlined struts received trunnion pins located outboard and in the center of the end plates. Trailing arms, extending 12" aft of the center of the plates, were fastened to a cross piece which in turn was connected to a third streamlined strut. The three struts passed through the tunnel floor to the balance. (See Figs. 3 and 6)

The tests were conducted in the Merrill Low Speed Wind Tunnel, described in Appendix A. All of the measurements were made at a dynamic pressure, $q = 25$ lbs/ft^2 and at a Reynolds Number, $R = 0.71 \times 10^6$; with the exception of the tests to determine the tare coefficients of the supports and endplates. For the tares, $q = 20$ lbs/ft^2 was used due to large vibrations encountered with the airfoil removed at higher speeds.

It would have been desirable to have made the tests with a considerably larger q, but it was felt that the large oscillatory forces observed in the stalled condition would be destructive to the balance. Considerable difficulty was encountered, even at $q = 25$ lbs/ft^2, with large vibrations at the stall. This was finally overcome by locking the moment-measuring lever arm of the balance at the particular angle of attack under study. The device used for this is shown in Fig. 5b. This procedure unfortunately prevented measuring the pitching moment.

The simple expediency of removing the airfoil from between the endplates as a method for determining the tares, gives results of highly questionable accuracy, since the effect of mutual interference is not included. It was felt that this error could be tolerated in a qualitative comparison, because the effect is small in the lift component and confined primarily to drag. The error should not be significantly different between

the several configurations.

The test work was done in three general categories:

(1) Force polar runs were made for each configuration, varying the retraction of the nose piece. The slot closed condition was simulated by covering the slot with 0.003" - thick cellophane tape. The basic airfoil was simulated by extending the leading edge to give the full 10" chord and taping the slot. There were slight irregularities of the surface at the junctures between top and bottom pieces and the nose piece. These irregularities were covered with tape, but tests made with and without the tape showed no significant differences. The split flap was simulated by bolting a flap, cut from 0.041" - thick material, to the lower surface at a point which would correspond to the hinge line. (See Fig. 5c)

(2) A static pressure survey was conducted over the upper surface of several representative configurations and on the basic airfoil using the probe described in Appendix B. Fig. 5d shows the installation of the probe and Fig. 7 shows the probe in detail. The pressure was measured on an alcohol micromanometer referenced to free-stream static pressure. Free-stream pressure was assumed to be the pressure taken at orifices located at the entrance to the test section. The difference between this and the atmospheric pressure outside the tunnel was in the order of one cm. of alcohol.

(3) A limited tuft survey was made on several representative configurations with a single-tuft probe. This probe consisted of a single strand of cotton thread, about 3/8" long, attached to a slender rod.

III. MODEL CONFIGURATION AND NOTATION

The following symbols are used to denote the model configuration. See Fig. 1 for layout of section profiles and Fig. 4 for layout of slots.

I - Basic circular-arc airfoil.

II - Lower surface leading-edge staggered 5.9% of chord aft of upper surface leading edge.

III - Lower surface leading-edge staggered 1.9% of chord aft of upper surface leading edge.

IV - No stagger between upper and lower surfaces.

A - Slot 'A'.

B - Slot 'B'.

C - Slot 'C'.

D - Slot 'D'.

E - Slot closed (covered with cellophane tape).

f - As subscript, 20% chord split flap deflected 60°.

(xx.xx) - Retraction of nose piece, distance in percent of original chord.

Example: $III_f C(9.06)$ - configuration III, with flap, with slot 'C', retracted 9.06%.

The following notation and definitions are used:

b - model span, = 24".

c - basic chord, = 10".

C_L - section lift coefficient, = L/qS.

$C_{L_{max}}$ - maximum lift coefficient.

C_D - section drag coefficient, = D/qS.

C_p - pressure coefficient, = $\Delta p/q$.

D - drag force, lbs.

L - lift force, lbs.

ℓ - characteristic length, ft.

Δp - increment of static pressure, = $p_{\text{free stream}} - p_{\text{surface}}$.

q - wind tunnel dynamic pressure, = $1/2\rho V^2$.

R - Reynolds number, = $V\ell/\nu$.

S - model wing area, = 1.667 ft^2.

V - wind tunnel free-stream velocity.

α - section angle of attack, degrees.

ρ - air density, slugs/ft^3.

ν - kinematic viscosity, ft^2/sec.

IV. RESULTS AND DISCUSSION

The results of the force measurements and pressure surveys are presented in Figs. 8 through 26. Table I shows a summary of $C_{L_{max}}$ for all configurations and serves as an index to the figures. In order to make a true comparison with the basic airfoil, the coefficients were computed using the original 10" chord. If the reduced chord, due to retraction, is used in calculating the coefficients, higher values result which give a false picture of the effectiveness as a high-lift device. This is illustrated in Fig. 17.

Force coefficients have been corrected only for the tares of model supports and end-plates. Corrections for downwash and tunnel walls were not attempted because of the unknown effect of the end-plates. Corrections to dynamic pressure due to blockage were negligible.

The results are discussed individually by configuration as follows:

I. Lift.

(a) Configuration I. Fig. 8. The basic airfoil had a $C_{L_{max}}$ of 0.725 at an angle of attack of 10°. In comparison some NACA data shows, for the same airfoil section, a $C_{L_{max}}$ of 0.73 at an angle of attack of 8° with $R = 6 \times 10^6$ and a $C_{L_{max}}$ of 0.75 at an angle of attack of 10° with $R = 2 \times 10^6$ (Refs. 3 and 8 respectively). Evidently, there is little variation with Reynolds number except in the stalling angle. There was an unusual variation in the slope of the lift curve at low angles of attack. A lower slope existed between -2° and 2° changing to a larger slope after 2°. The same variation is found on close examination of the results of Ref. 8. No explanation can be given for this, except that it may be associated with the laminar separation which is just beginning at low angles of attack. Since the prime interest of this test was maximum lift, the phenom-

enon was not investigated further.

(b) Configuration IIA. Fig. 8. With increasing amounts of retraction a loss in maximum lift proportional to the loss in area was observed until the leading edge was retracted to 9.06%. At this point the maximum lift abruptly increased to a value about equal to the basic airfoil and the stall was delayed until an angle of attack of 12° was reached. (When retracted to the 9.06% point, the leading edge is approximately 1/32" ahead of the leading edge of the upper surface.) For all amounts of retraction greater than 9.06%, the maximum lift was considerably reduced from the basic airfoil and almost constant. The loss in this case was about 20%, which is roughly a 10% greater loss than would be expected due to loss in area.

The variation of $C_{L_{max}}$ with retraction is best shown in Fig. 16. This plot shows the variation from the basic airfoil for all configurations. The dashed line represents an assumed linear loss in maximum lift from the basic airfoil, proportional to the loss of area and calculated as follows:

$$-\Delta C_{L_{max}} = (\text{retraction})(0.725), \quad \text{retraction} < 9.4\%$$
$$= (0.94)(0.725), \quad \text{retraction} > 9.4\%$$

(c) Configuration IIIA. Fig. 9. Results were essentially the same as configuration IIA except that the abrupt increase above the linear loss at 9.06% was not as great. Because the maximum lift was apparently sensitive to small changes near this point, positions a few hundreths of a percent to each side of 9.06% were tested to find an optimum position. In every case the lift was less than at 9.06%.

(d) Configuration IIIB. Fig. 10. Inspection of the geometry involved at the 9.06% point revealed that the inlet space to the slot was very small. In an effort to determine whether the increase in lift at this

point was due to the size of the slot entrance, which varied according to the retraction, or to retraction alone, the slot was modified as shown in Fig. 4. The slot gap was increased about 50% and the contour was milled down to increase the inlet area. The results were approximately the same as before until the 9.06% point was reached where the maximum lift decreased sharply. The maximum lift at points past 9.06% was also less but the stall was considerably smoother and the lift curves were almost horizontal past the stall.

(e) Configuration IIIC. Figs. 13 and 14. From the above tests it was apparent that there was some inter-action between the relative position of the nose piece and the inlet area and/or slot gap. The slot gap was reduced to the original dimension and the contour further modified to increase the inlet area (see Fig. 4). In this configuration the model was tested at only two retracted positions, 9.06% and 20%. $C_{L_{max}}$ obtained at the 9.06% point was slightly better than configuration IIIA and somewhat less than IIA. At the 20% point, the results were similar to the IIA configuration and did not produce the 'flat' stall as in IIIC.

(f) Configuration IIID. Figs. 13 and 14. The slot gap was reduced approximately 30% and the contour was unchanged. Again, only two positions were tested, 9.06% and 20%. The results were essentially the same as IIIC with slight increases in maximum lift at both points.

(g) Configuration IVD. Fig. 11. Approximately the same values of maximum lift were obtained as with configuration IIA. The lift curves at the stall were smoother for every retracted position and the stalling angle of attack at 9.06% was extended to 12.5°.

The effect of the various slots and different amounts of stagger, with the leading edge retracted 9.06% and 20%, is shown in Figs. 13

and 14. Generally, stagger has little apparent effect while the size and shape of the slot appears to change $C_{L_{max}}$ a significant amount.

(h) Slot closed configurations. Fig. 12. The effect of not having a slot was to reduce the maximum lift, except on configuration IVD (9.06). The stalling angle of attack was reduced to 8° for retractions past 9.06% with the slot closed. The only exception to this general effect was the configuration IVE(9.06), which had a lift curve almost identical to the corresponding open-slot configuration. This is inconsistent with the other configurations at 9.06%, where an increase in maximum lift above the linear loss was not observed with the slot closed. This point will be discussed further in a following paragraph.

(i) Trailing edge flap configuration. Fig. 15. It was felt that advantage might be taken of the increase in angle of attack for maximum lift found for the configuration IVD (9.06) by using it in combination with a trailing-edge flap. The results with a 20% chord, split flap deflected 60° were quite the opposite. The flapped configuration with 9.06% retraction stalled at the same angle of attack as the flapped, basic airfoil and produced less maximum lift. The 20% retracted position with flap stalled at one degree less angle of attack than the basic airfoil and had considerably less maximum lift.

II. Drag.

Drag polars of configurations IIA, IIIA, and IVD are shown in Figs. 18, 19 and 20. For simplicity only the representative positions, 9.06% and 20% retraction are shown. For the same C_L, the C_D of the retracted configurations was higher than the basic airfoil. $(C_L/C_D)_{max}$ was less than the value for the basic airfoil in every case. Configurations IVD (9.06) and IVE (9.06) had the least drag of the retracted configurations;

the polars of these two configurations closely approached that of the basic airfoil.

III. Upper Surface Pressure Distribution.

Figs. 21 through 26. Static pressure surveys were made on several representative configurations to determine the variation in pressure distribution and thereby, some indication of the type of flow. The general effect on the pressure distribution due to retraction was to cause a higher peak of negative pressure near the nose. The pressure increased rapidly after the negative peak. Aft of about 30% of the chord, the pressure gradient of the retracted airfoil was nearly the same as the basic airfoil.

Considerable variation was found in the pressures with and without the slot, and with different slots. The typical pressure distribution of configuration IIIC (Fig. 21) was a constant level from the nose to the slot, followed by a jump to a negative peak behind the slot and then a sharp positive gradient to about 20% chord. Aft of this point the gradient was similar to the basic airfoil. The IVD configuration was rather different. A large negative pressure peak occured at the nose followed by a sharp positive gradient reaching an opposite peak at the slot. Aft of the slot a second and smaller negative peak occurred followed by a gradient similar to IIIC and I.

Distribution of pressure with the slot closed not only varied from the corresponding configuration with the slot open, but with different basic configuration. The distribution of III with slot closed was relatively smooth and followed that of the basic airfoil. Comparison of the pressure distribution of IVD (9.06) and IVE (9.06) was of particular interest since these two configurations had the same lift curve. (See section (h).) Figs. 23 through 26 show that the pressure distribution was

essentially the same, slot open or closed, on IVD, the only difference being the irregularity at the slot with the slot open. In comparison with the overall shape of the pressure profile, the discontinuity with the slot open appears to be of little importance.

From the results of the pressure tests, it appears that there is little, if any, flow through the slot; and that all of the relative increase in lift at the 9.06% position is due to position of the nose piece.

III. Single-tuft Flow Survey.

A further attempt to determine the nature of the flow about the retracted configurations and slots was made using a single strand tuft attached to a slender probe.

The significant result from this investigation was that the gross flow about the retracted configurations was not greatly different from that of the basic airfoil. It was found that the laminar separation 'bubble' occurred as with the plain airfoil, and in about the same place. The extent of the separated region could be readily determined with the single-tuft, however precise regions were not mapped since the probe was hand-held. Strong vortex flow, in a direction such that reverse flow existed next to the surface, was indicated in the interior of the 'bubble'. The point of reattachment was roughly indicated by a region of confused flow approximately 5% of the chord in width. Behind this confused region there was an attached turbulent boundary layer and ahead of it, strong reverse flow. The point of reattachment apparently progressed aft with increasing angle of attack.

With the leading edge retracted 9.06%, the tuft indicated no flow through the slot on configurations IIID and IVD, from an angle of attack of 0° to about 6°. From 6° to approximately 1° less than the stalling

angle of attack, there was definite reverse flow through the slot. At the stall there was no apparent flow through the slot.

There was a slight indication of flow through the slot in the proper direction with the leading edge retracted 20% at the stall.

V. CONCLUSIONS

From the results of the investigation it may be concluded that:

(1) Retraction of the leading edge is not an effective high-lift device on a sharp-nosed airfoil, and in fact, is generally detrimental to maximum lift due to the combined effects of loss in wing area and increased deterioration of the flow with large amounts of retraction.

(2) The general type of flow about the retracted configuration and the type of stall remain unchanged from the basic airfoil.

(3) With a particular amount of retraction, in this case 9.06% of the chord, and in combination with either a certain slot configuration and/or stagger between upper and lower surfaces, the maximum lift is equal to the basic airfoil, but the stalling angle of attack is increased by 2°.

(4) The effect of stagger between upper and lower surfaces is negligible except with 9.06% retraction.

(5) The upper surface slot is beneficial to maximum lift; however the size of the slot is critical in obtaining the relative increase in lift at 9.06% retraction.

Pages 17 and 18 blank.

REFERENCES

1. Pollock, A.D. and Reck, F.F.: "A Study of Methods to Increase the Lift of Supersonic Airfoils at Low Speeds", Thesis, CIT, 1947.

2. Bacon, J.W.: "An Investigation of Blowing as a Method of Increasing the Maximum Lift of a Double-Wedge Airfoil", Thesis, CIT, 1947.

3. Nuber, R.J. and Chessman, G.A.: "Two-Dimensional Wind Tunnel Investigation of Six-Percent Symmetrical Airfoil Section With Leading and Trailing Edge High Lift Devices Deflected in Combination", NACA RM L9G20, 1949.

4. Rose, L.M. and Altman, J.M.: "Low Speed Experimental Investigation of a Thin, Faired Double-Wedge Airfoil Section with Nose and Trailing Edge Flaps", NACA TN 1934, 1949.

5. Wallace, R.W.: "Low Speed Investigation of a Double-Wedge Airfoil with Leading Edge Slat", Thesis, CIT, 1951.

6. Davidson, H.W.: "Lift Increase Obtained with Boundary Layer Suction on a 10% Double Wedge Airfoil with 20% Chord Leading and Trailing Edge Flaps", Thesis, CIT, 1951.

7. Loftin, L.K. and von Doenhoff, A.E.: "Exploratory Investigation at High and Low Subsonic Mach Number of Two Experimental Six Percent Airfoil Sections Designed to Have High Maximum Lift Coefficients", NACA RM L51F06, 1951.

8. Bursnall, W.J.: "Experimental Investigation of the Effects of Vortex Generators on the Maximum Lift of a 6-percent Thick Symmetrical Circular-arc Airfoil Section", NACA RM L52G24, 1952.

9. McCullough, G.B. and Gault, D.E.: "Examples of Three Representative Types of Airfoil Section Stall at Low Speed", NACA TN 2502, 1951.

10. Willmarth, W.W.: "The Lift of Thin Airfoils at High Subsonic Speeds", Thesis, CIT, 1954.

APPENDIX A

DESCRIPTION OF THE MERRILL WIND TUNNEL

The Merrill Wind Tunnel at the California Institute of Technology is a conventional, single return, closed-circuit type approximately 110' long, with a six-to-one contraction ratio. The test section is rectangular, 32" by 45". At the time of these tests three anti-turbulence screens were installed between the settling chamber and entrance cone. A three-bladed propeller is driven by a 75 hp constant speed AC motor. Wind velocity, variable between 0 and 180 mph, is controlled by varying the propeller pitch through a Curtis-Wright electric propeller hub.

Force measurements were made on a mobile, three component, beam type, manual balance. (See Fig. 5b) Indicated error in repeatability of measurements was $\pm$ 0.04 lbs. in lift or drag, which corresponds to an error of approximately $\pm$ 0.001 in the force coefficients computed for the model at a dynamic pressure of 25 psf.

APPENDIX B

STATIC PRESSURE SURVEY PROBE

It was found convenient by Willmarth (Ref. 10) to employ a traversing static pressure probe to measure the surface pressure on a thin airfoil. The basis for use of such probes is that the static pressure is constant through the boundary layer in a direction normal to the surface and that the flow outside the boundary layer is irrotational. The boundary condition that the surface curvature is small, applied to these assumptions gives the linearized result that the normal pressure gradient is small.

While the circular-arc model was under construction several static pressure probes similar to Willmarth's were made and tested on Wallace's model (Ref. 5). The details of the probe used on the circular-arc are shown in Fig. 7 and the installation is shown in Fig. 5d. Since there was to be no means of axial orientation of the probe, three pressure taps, circumferentially spaced 120°, were used. These pressure taps were the same size as the orifices on Wallace's model, 0.0135" in diameter. The probe was mounted approximately mid-span on the model and held flush by a wire attached to the tip of the probe and extending upstream through vertical positioning wires; thence passing through the bottom of the tunnel. A rubber tube and a wire were fitted to the aft end of the probe and carried outside of the tunnel through a larger, plastic tube. By means of the fore and aft wires the probe could be traversed over the chord with the tunnel in operation.

Pressures measured by the probe were compared to pressures measured by the model's surface orifices at the same chordwise station. The indicated difference between the two pressures was less than the experimental

error except very near the leading edge where the difference was in the order of 5 to 10% of total reading referred to atmospheric. The larger error near the nose is believed to be aggravated, to some extent, by lack of precision in setting the probe taps in the exact chordwise station of the model orifices. Due to the steep pressure gradient at the nose, an error in position is greatly magnified. Yawing the probe up to about 5° and different random, axial orientations made no significant difference in the indicated error.

The static pressure probe has two distinct advantages: the complex installation of surface orifices, difficult in thin models, is avoided; and pressures at an infinite number of stations can be measured. Due to the high damping of the small pressure taps and lines, the probe is not sensitive to fluctuating pressures. The primary disadvantage of the system is the increased tunnel operating time required to make a series of measurements. This time is further increased by the damping. Up to two or three minutes were required to establish a steady reading upon change of station.

TABLE I

SUMMARY OF RESULTS AND INDEX TO FIGURES

Run No.	Configuration	$C_{L_{max}}$	$\alpha_{C_{L_{max}}}$	ΔC_L	Fig. No.
1	I	.725	10	-	8
2	IIA (6.25)	.68	10	-.045	8
3	(9.06)	.73	12	.005	8,13
4	(9.375)	.575	10	-.15	8
5	(11.56)	.563	10	-.162	8
6	(14.06)	.593	10	-.132	8
7	(16.56)	.593	10	-.132	8
8	(20.00)	.586	10	-.139	8,14
9	IIIA (3.75)	.692	10	-.033	9
10	(6.25)	.674	10	-.051	9
11	(8.335)	.670	10	-.055	9
12	(9.06)	.683	11	-.042	9,13
13	(9.373)	.586	10	-.139	9
14	(9.685)	.580	10	-.145	9
15	(10.31)	.553	10	-.172	9
16	(11.56)	.564	10	-.161	9
17	(14.06)	.582	10	-.143	9
18	(16.56)	.590	11	-.135	9
19	IIIB (3.75)	.692	10	-.063	10
20	(6.25)	.674	10	-.051	10
21	(7.50)	.666	10	-.059	10

TABLE I (Continued)

Run No.	Configuration	$C_{L_{max}}$	$\alpha C_{L_{max}}$	ΔC_L	Fig. No.
22	IIIB (9.06)	.600	10	-.125	10,13
23	(11.56)	.564	11	-.161	10
24	(14.06)	.557	11	-.168	10
25	(20.00)	.536	10	-.189	10,14
26	IIIC (9.06)	.692	11	-.033	13
27	(20.00)	.596	10	-.129	14
28	IIID (9.06)	.710	12	-.015	13
29	(20.00)	.593	10	-.132	14
30	IIIE (3.75)	.693	10	-.032	12
31	(6.25)	.675	10	-.05	12
32	(9.06)	.585	9	-.14	12,13
33	(10.31)	.554	8	-.171	12
34	(11.56)	.554	8	-.171	12
35	(16.56)	.554	8	-.171	12
36	(20.00)	.563	9	-.162	12,14
37	IVD (3.75)	.694	10	-.031	11,13
38	(6.25)	.673	10	-.052	11
39	(9.06)	.721	12.5	-.004	11
40	(9.375)	.581	10	-.144	11
41	(11.56)	.580	10	-.145	11
42	(20.00)	.55	9	-.175	11,14
43	IVE (9.06)	.722	12	-.003	12
44	(20.00)	.559	9	-.166	12
45	I_f	1.630	6	.905	15
46	IV_fD (9.06)	1.489	6	.764	15
47	(20.00)	1.375	6	.650	15

TABLE I (Continued)

Configuration		Fig. No.
All	$C_{L_{max}}$ plotted vs. retraction	16
IVD	Difference in C_L based on 10" chord and reduced chord	17
IIA	Drag polar	18
IIIA	Drag polar	19
IVD	Drag polar	20
I IIIC(20.00) IVD (9.06)	Pressure distribution at $C_{L_{max}}$	21
IIIC(20.00) IIIE(20.00)	Pressure distribution at $C_{L_{max}}$	22
IVD (9.06)	Pressure distribution at $\alpha = 0^\circ$	23
IVE (9.06)	$\alpha = 4^\circ$	24
	$\alpha = 8^\circ$	25
	$\alpha = 12^\circ$	26

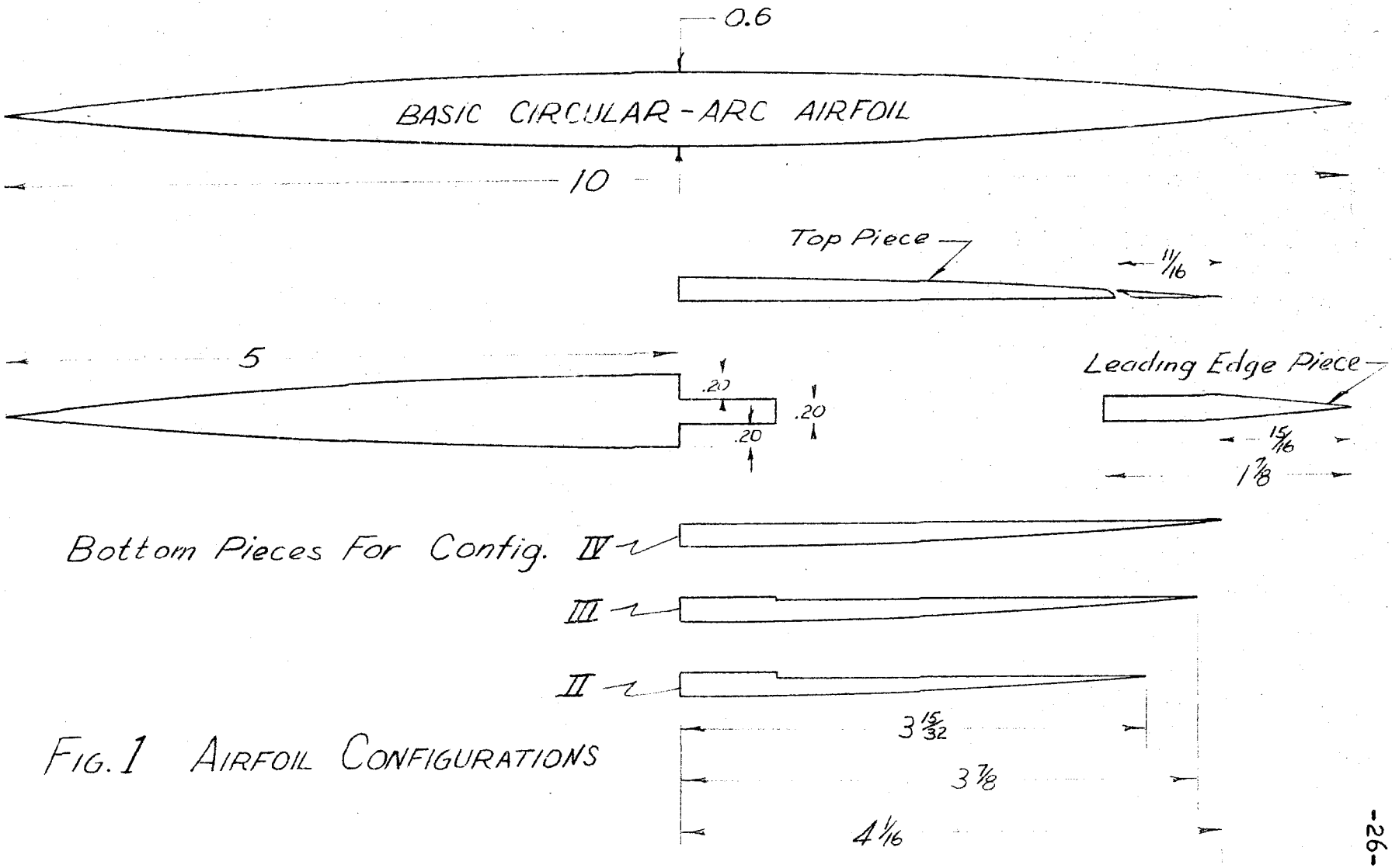

FIG. 1 AIRFOIL CONFIGURATIONS

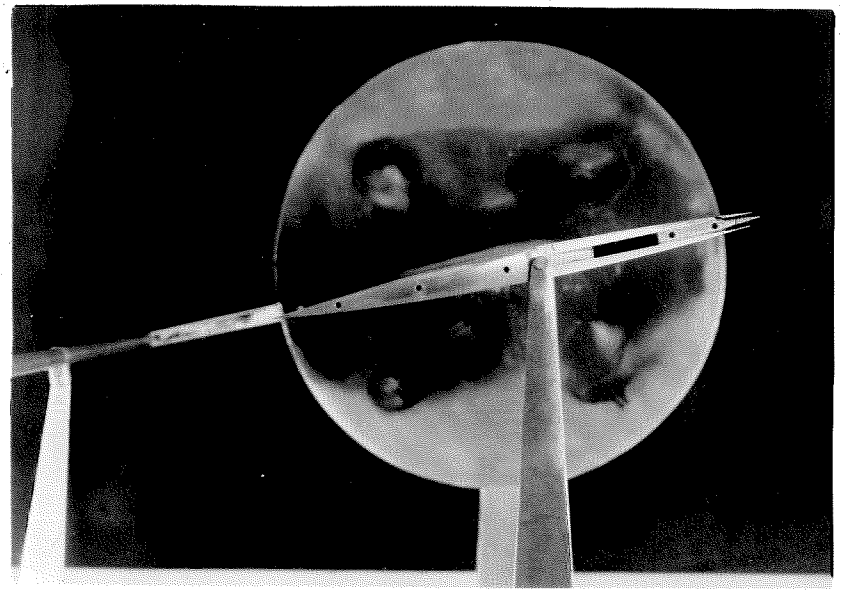

Fig. 2 Endplate removed showing model profile. Configuration IIIC(9.06).

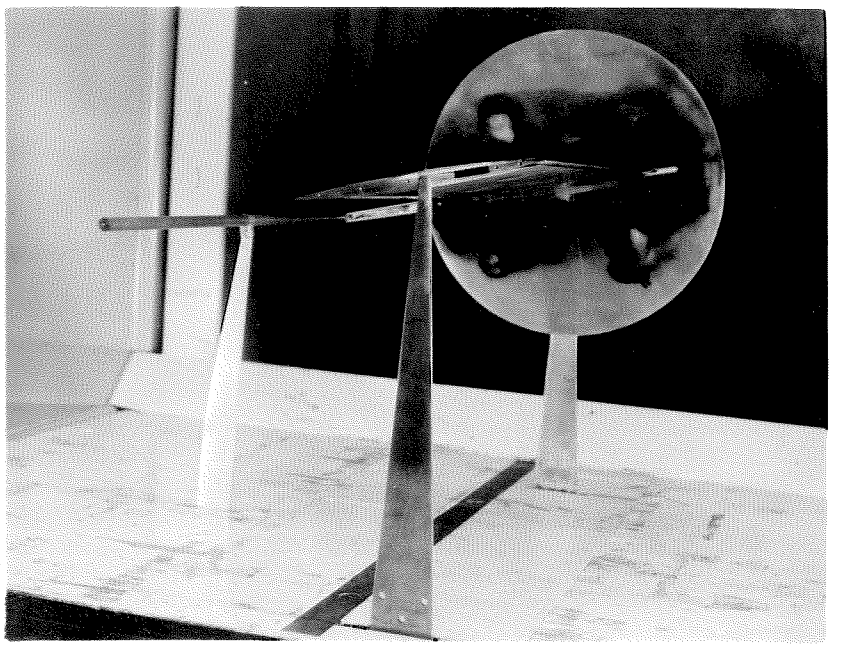

Fig. 3 Three point suspension system.

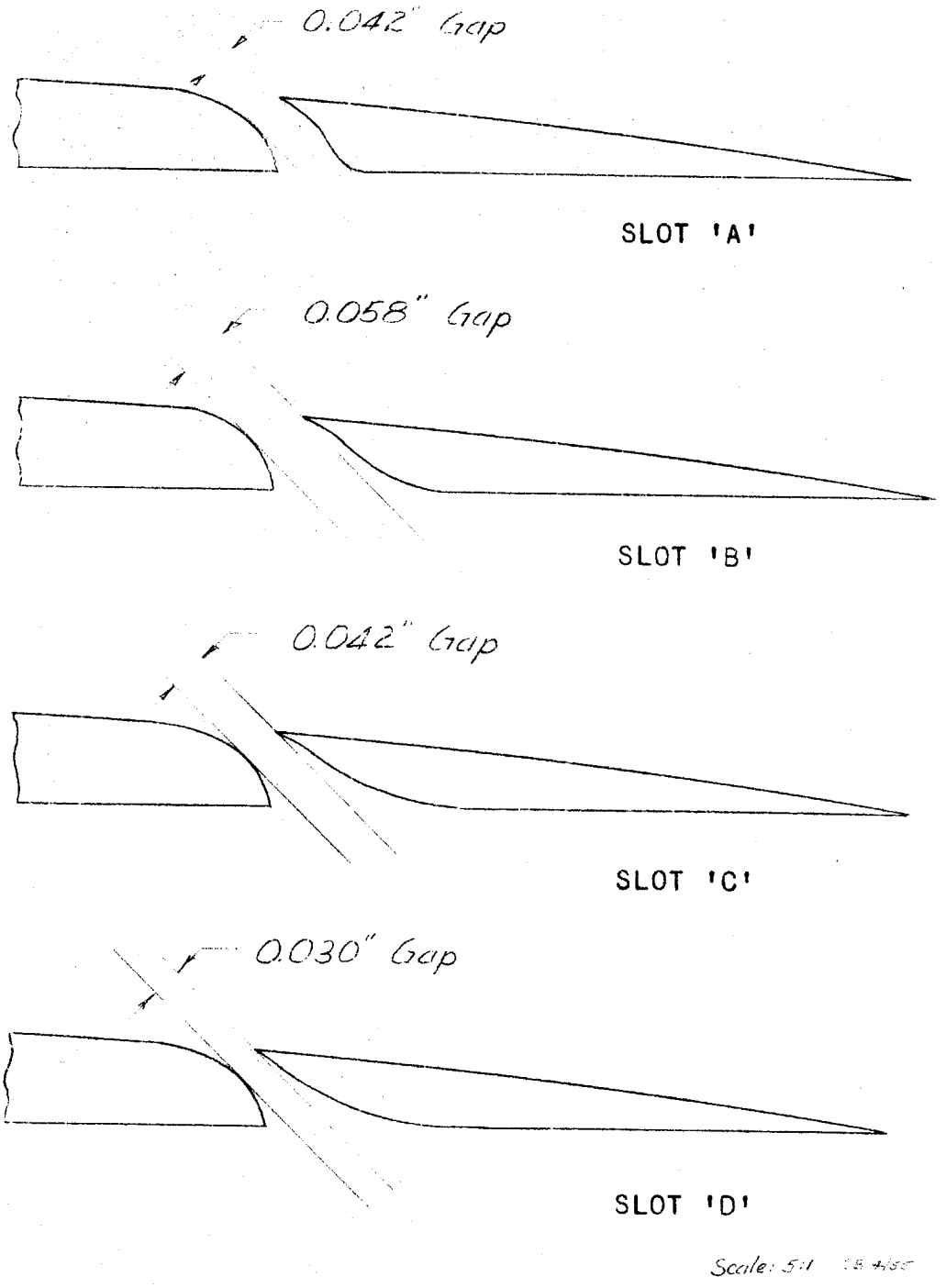

FIG. 4 - SLOT CONFIGURATIONS

(a) End view from above showing spanwise slot.

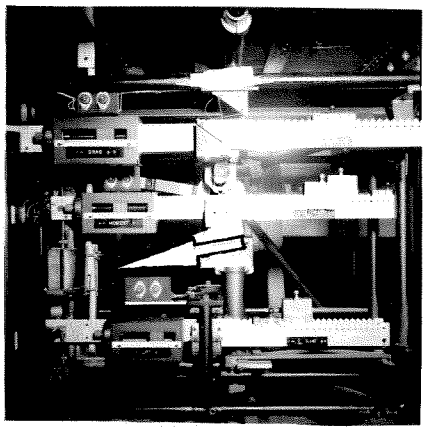

(b) Arrow indicates locking device used to restrain pitching moment arm.

(c) Model with 20%, split flap, deflected 60°.

(d) Static pressure probe installation.

Figure 5.

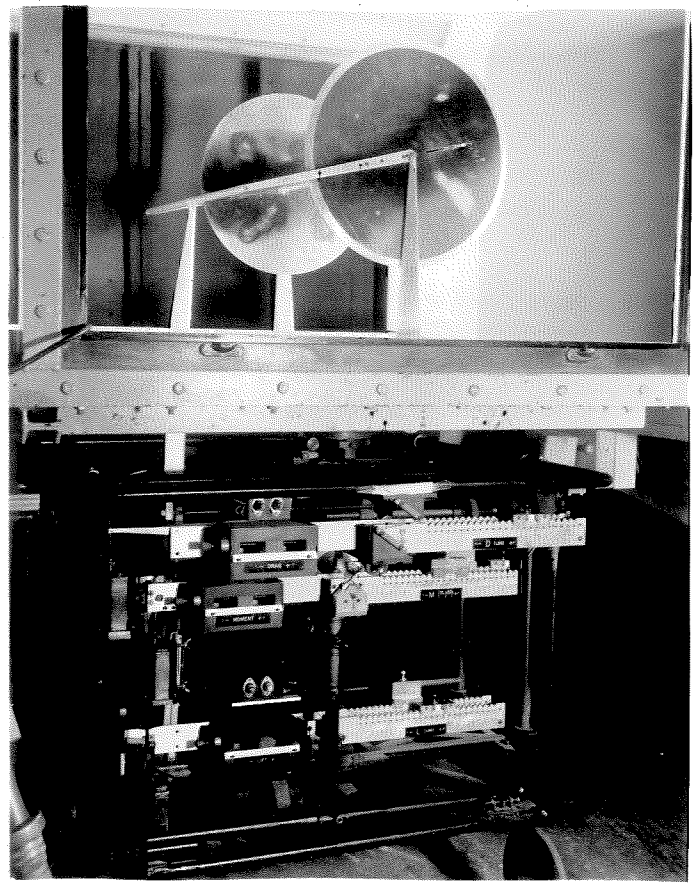

Fig. 6 Installation of model and mobile balance.

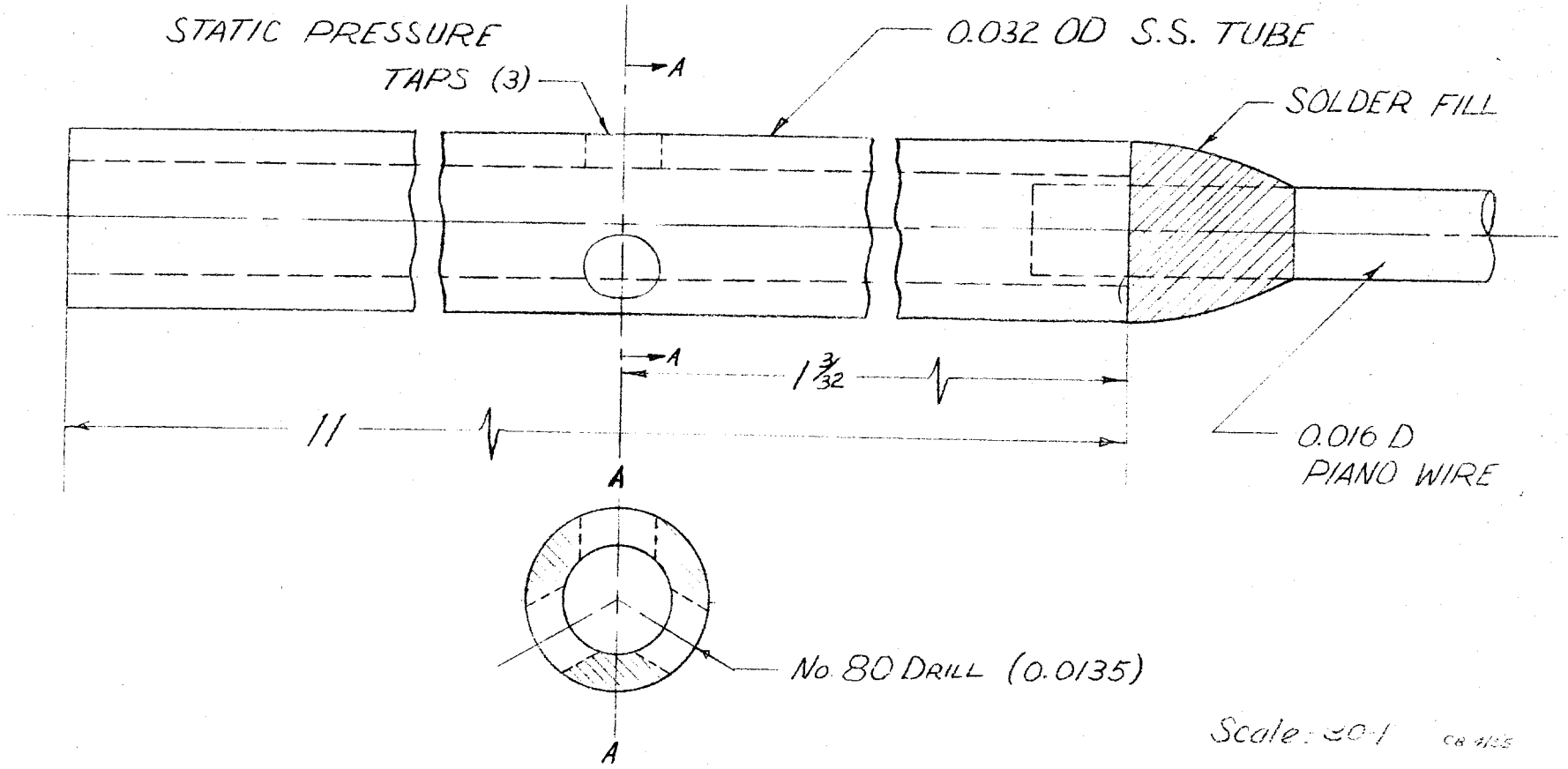

Fig. 7 - Static pressure survey probe.

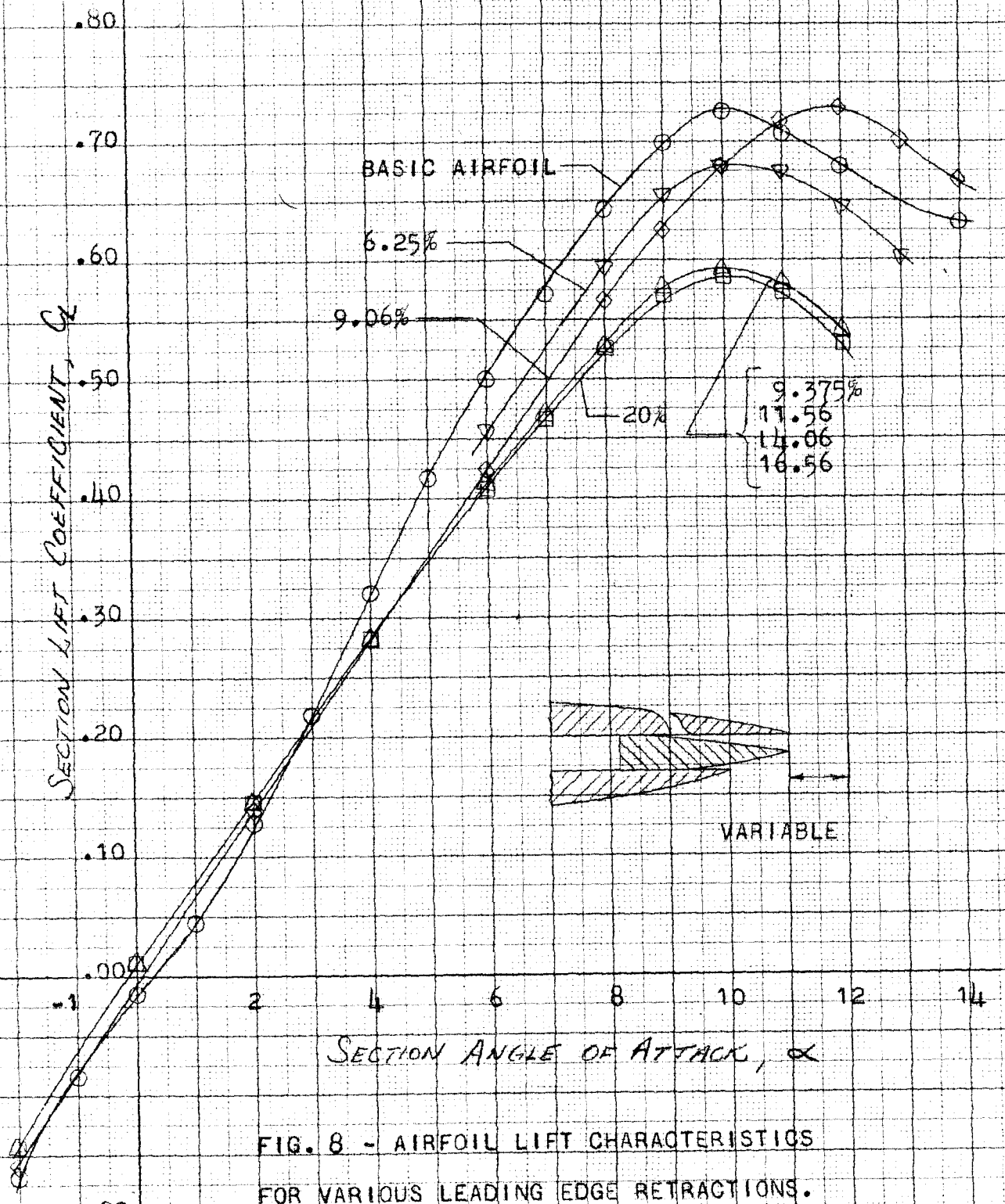

FIG. 8 - AIRFOIL LIFT CHARACTERISTICS FOR VARIOUS LEADING EDGE RETRACTIONS. CONFIGURATION 11. SLOT 'A'.

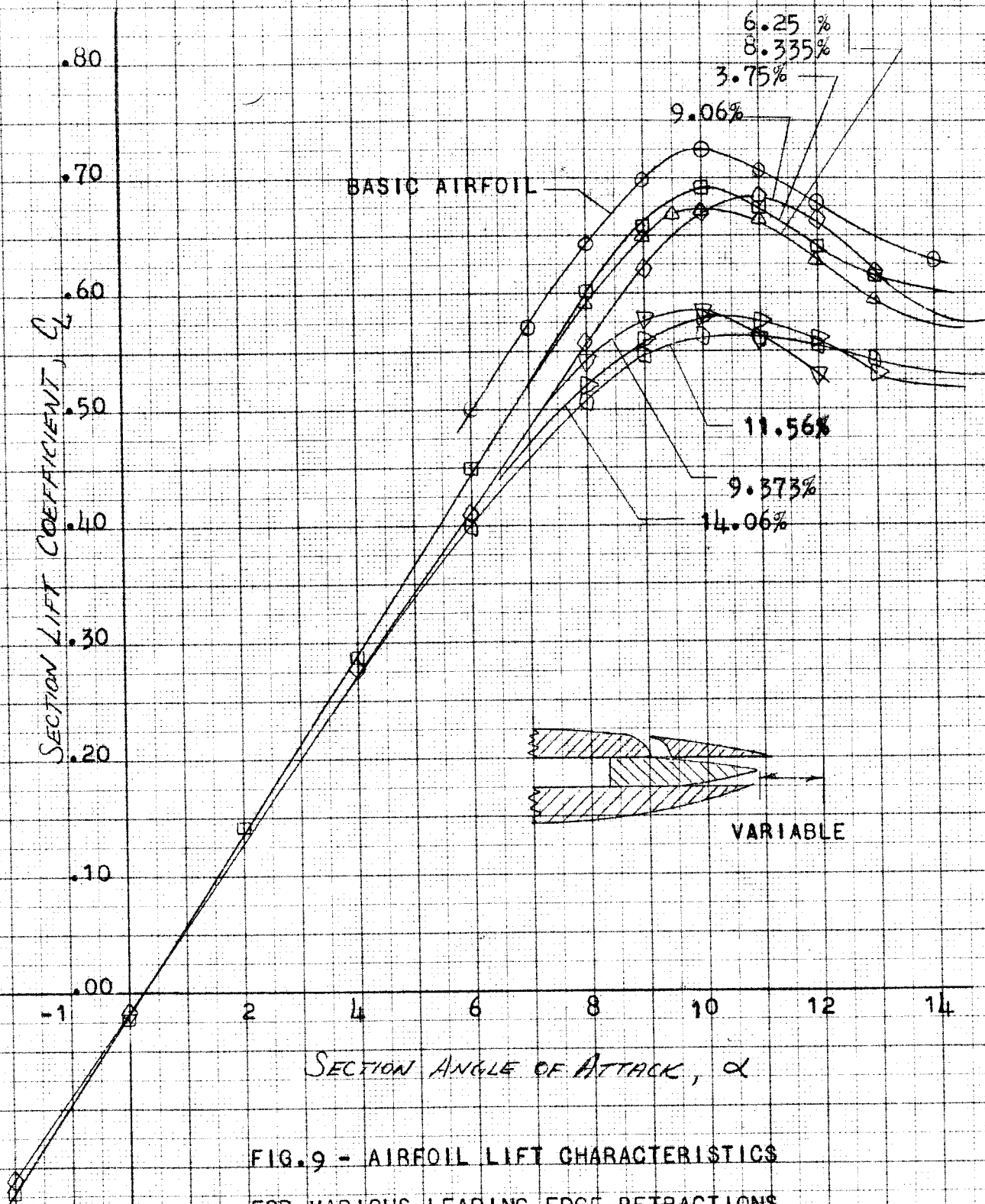

FIG. 9 - AIRFOIL LIFT CHARACTERISTICS FOR VARIOUS LEADING EDGE RETRACTIONS. CONFIGURATION III. SLOT 'A'.

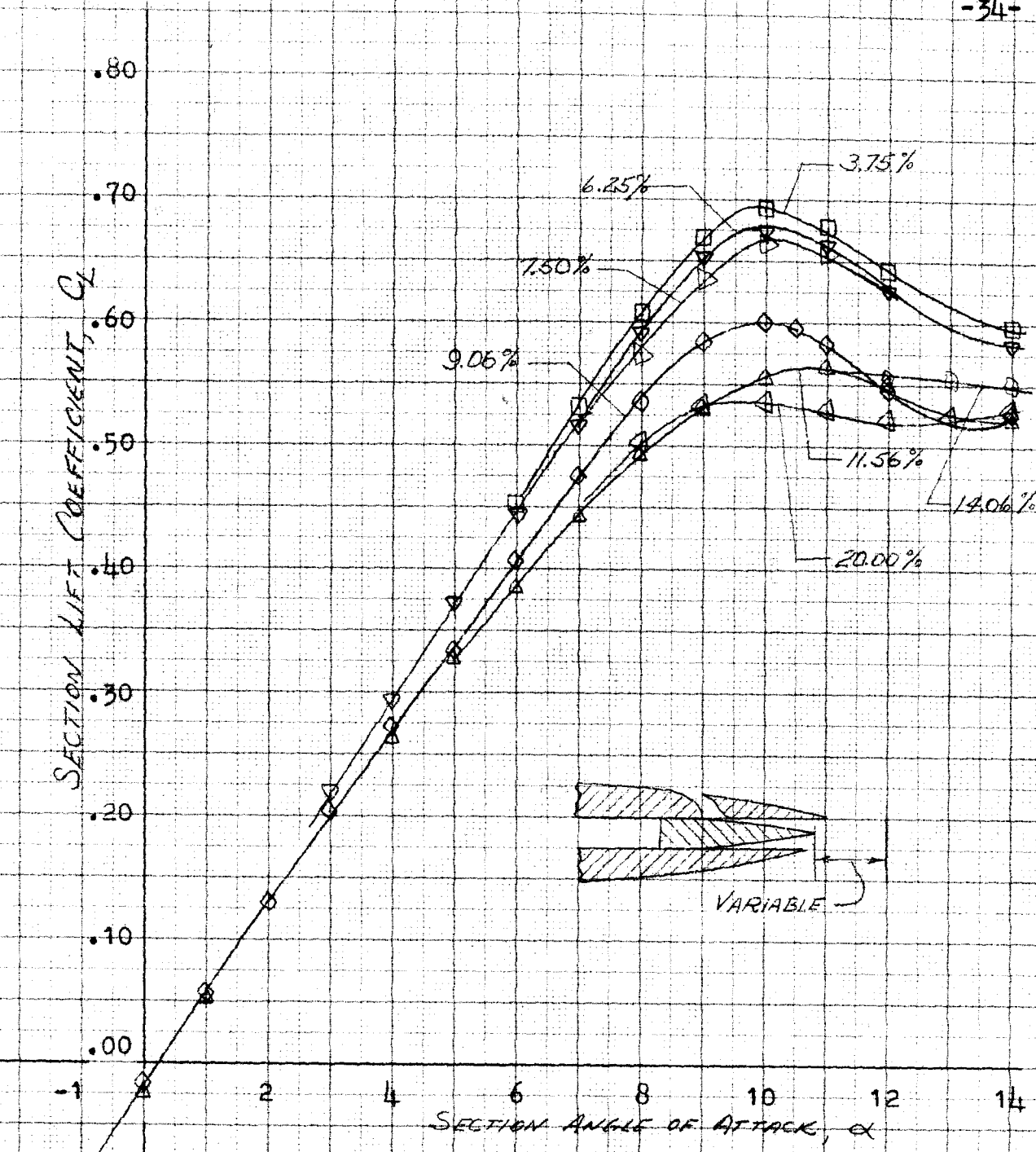

FIG. 10 - AIRFOIL LIFT CHARACTERISTICS FOR VARIOUS LEADING EDGE RETRACTIONS, CONFIGURATION IIIB

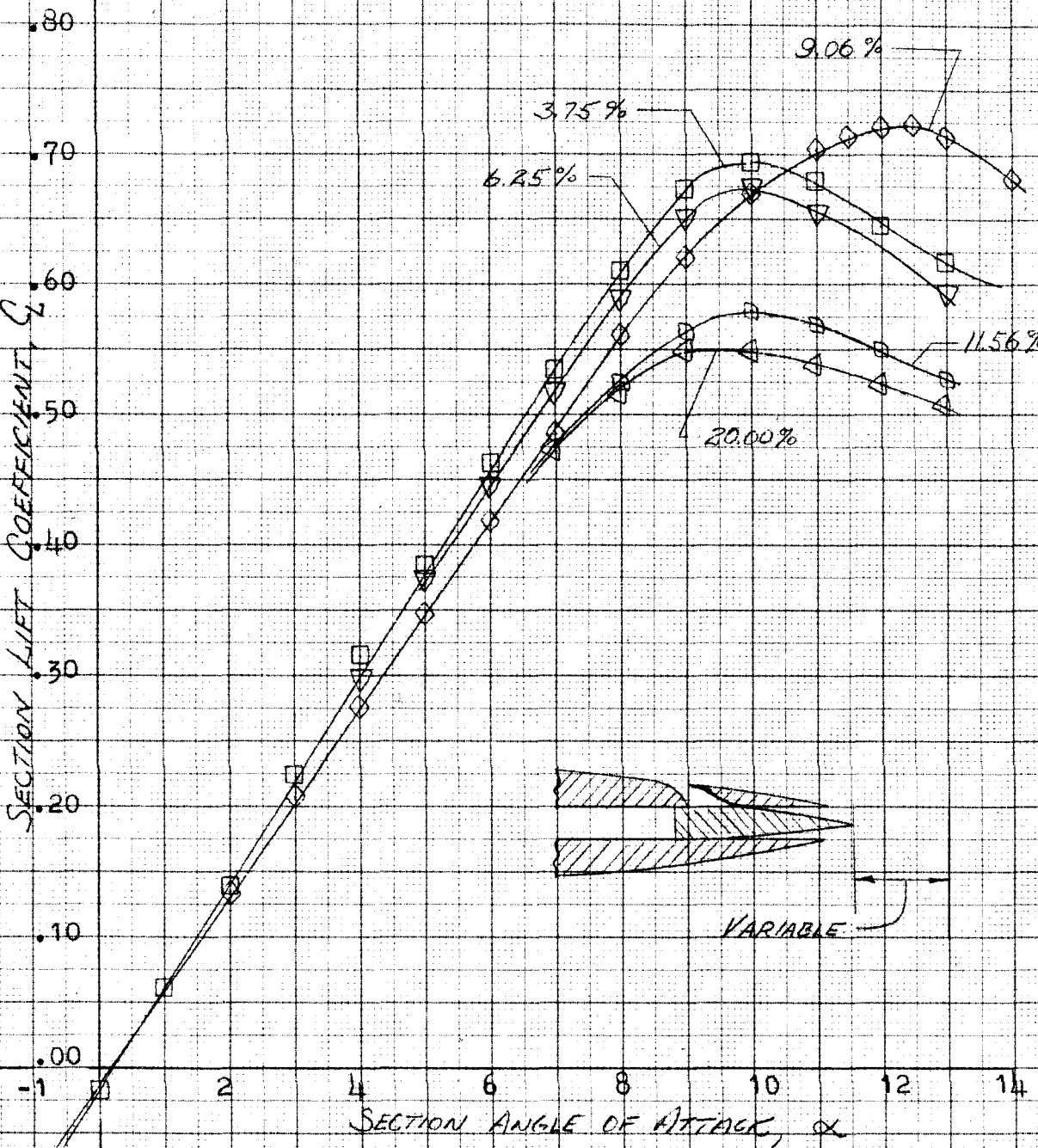

FIG. 11- AIRFOIL LIFT CHARACTERISTICS FOR VARIOUS LEADING EDGE RETRACTIONS. CONFIGURATION IV D

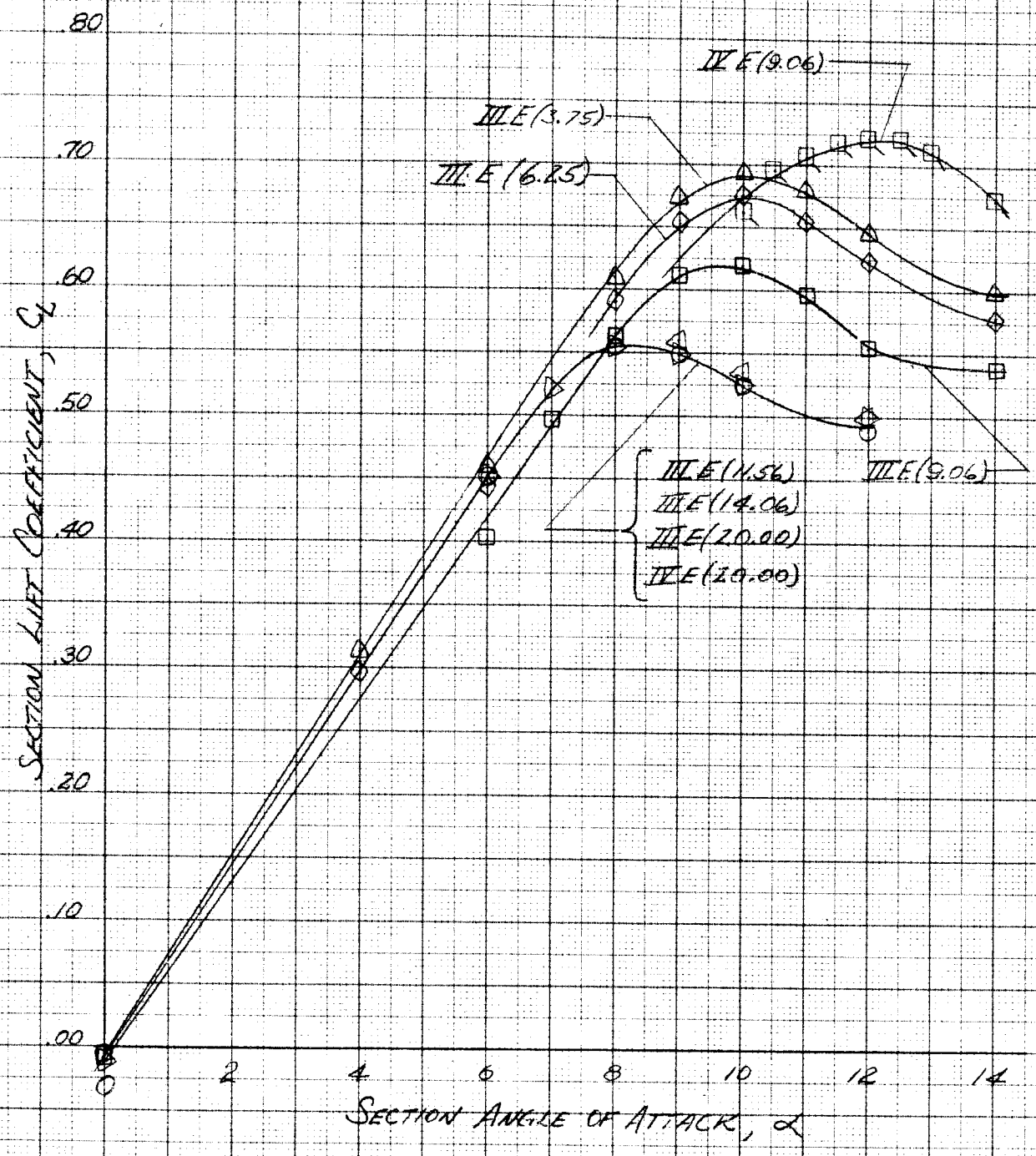

FIG. 12 AIRFOIL LIFT CHARACTERISTICS

SLOT CLOSED, VARIOUS RETRACTIONS

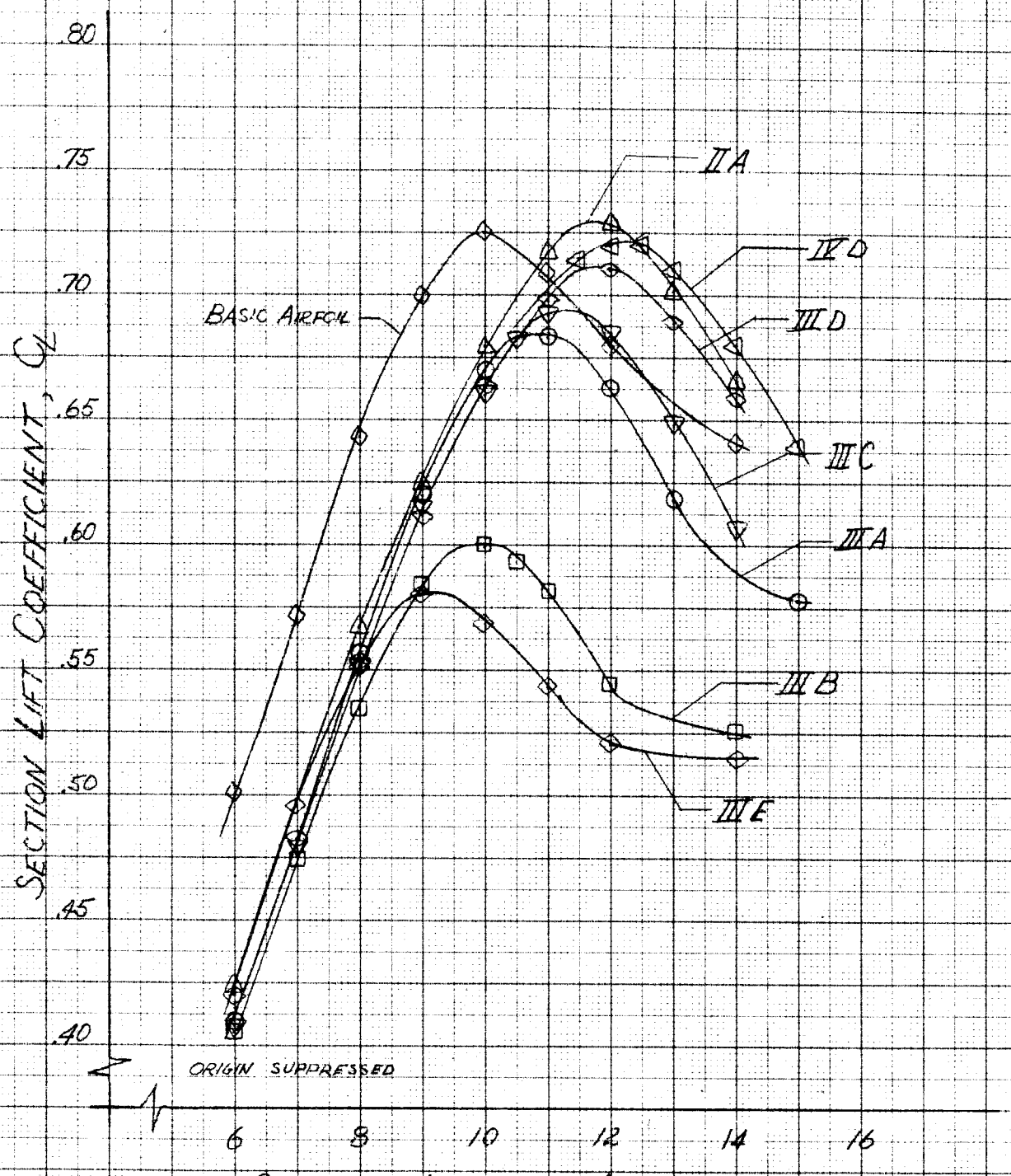

FIG. 13 VARIATION OF MAXIMUM LIFT WITH DIFFERENT SLOT CONFIGURATIONS, LEADING EDGE RETRACTED 9.06 %.

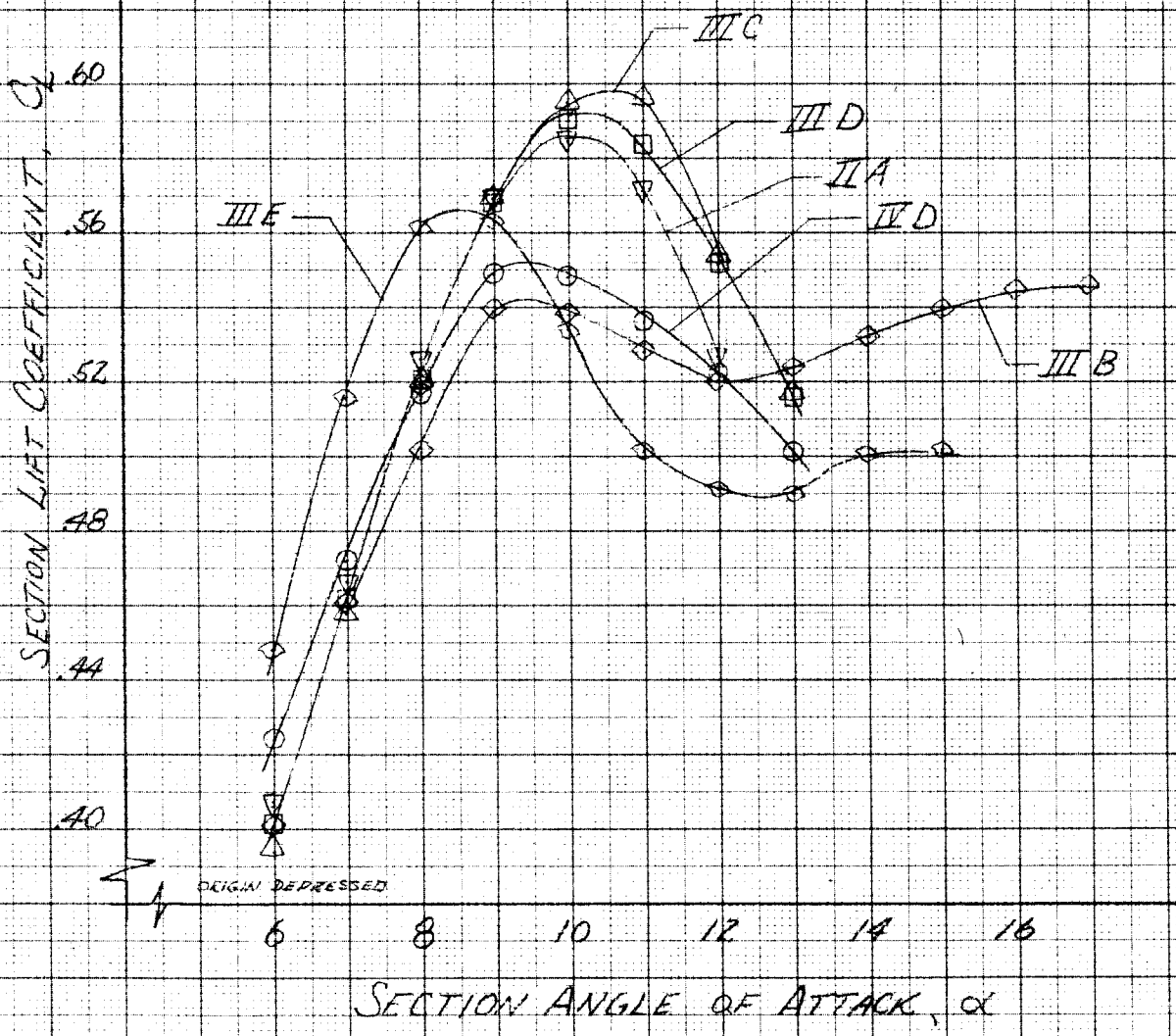

FIG. 14 VARIATION OF MAXIMUM LIFT WITH DIFFERENT SLOT CONFIGURATION, LEADING EDGE RETRACTED 20 %.

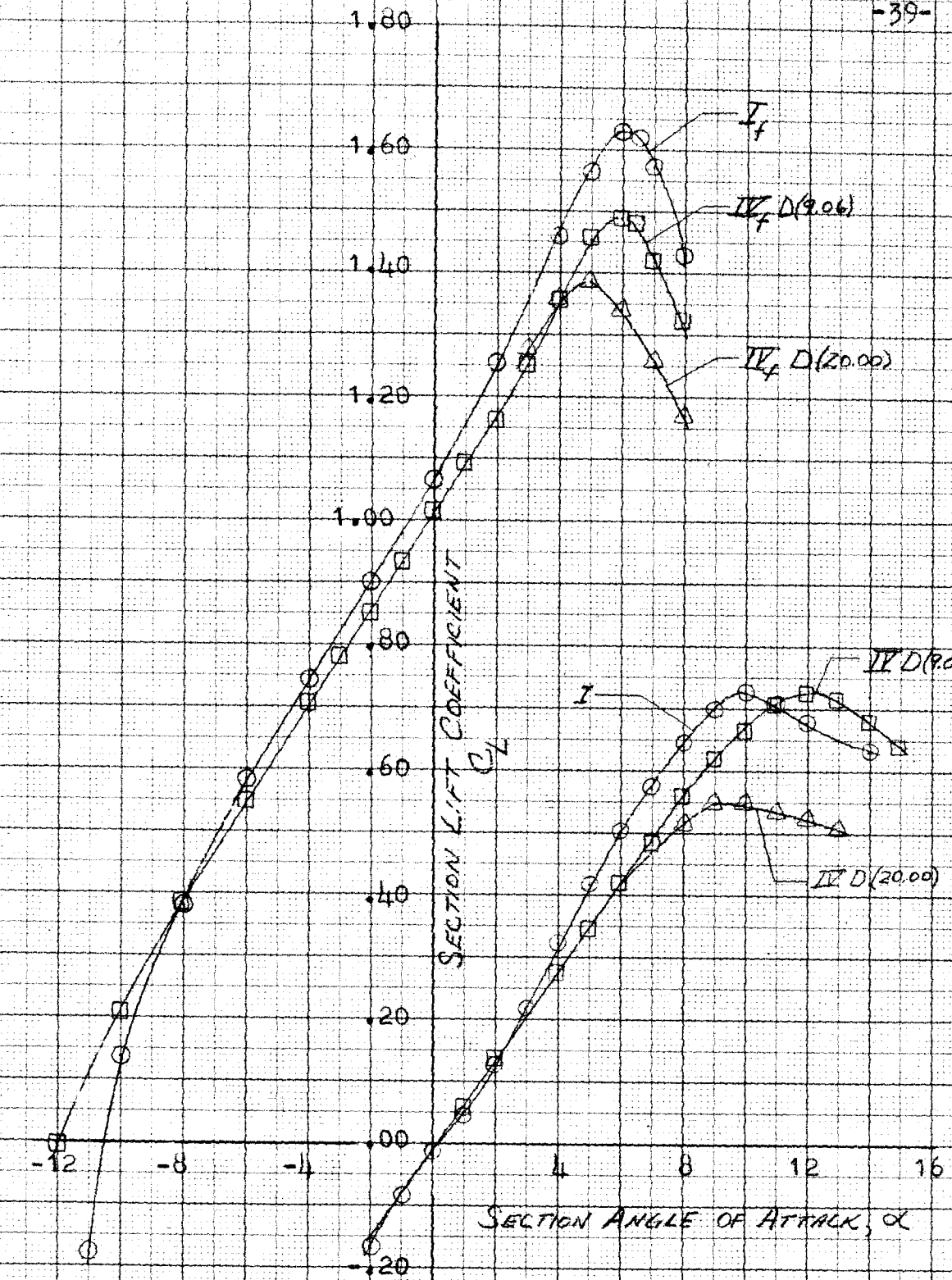

FIG. 15 LIFT CHARACTERISTICS WITH AND WITHOUT 20% CHORD SPLIT FLAP, DEFLECTED 60°. CONFIGURATIONS I AND IV D

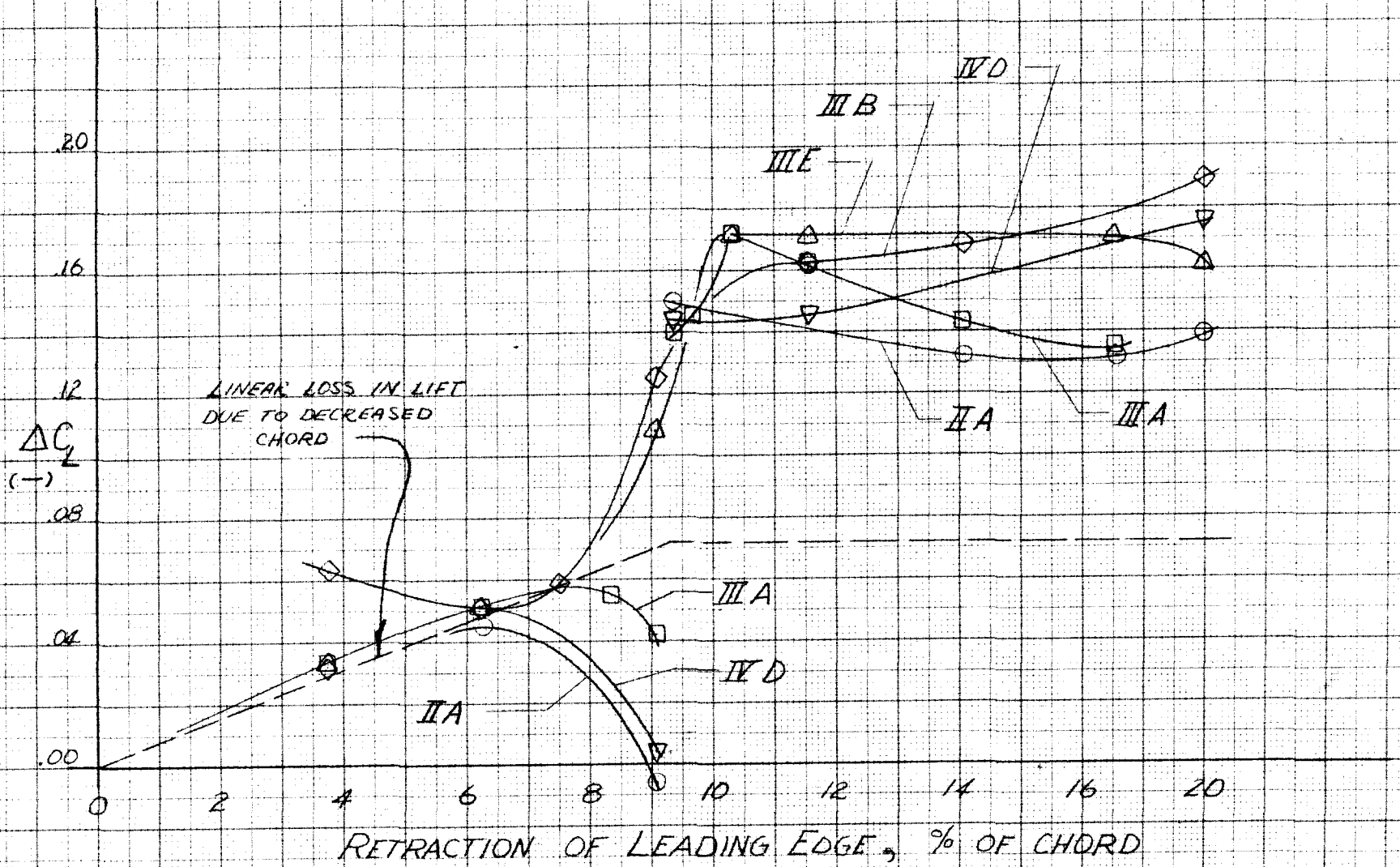

FIG. 16 VARIATION OF $C_{L_{MAX}}$ WITH RETRACTION

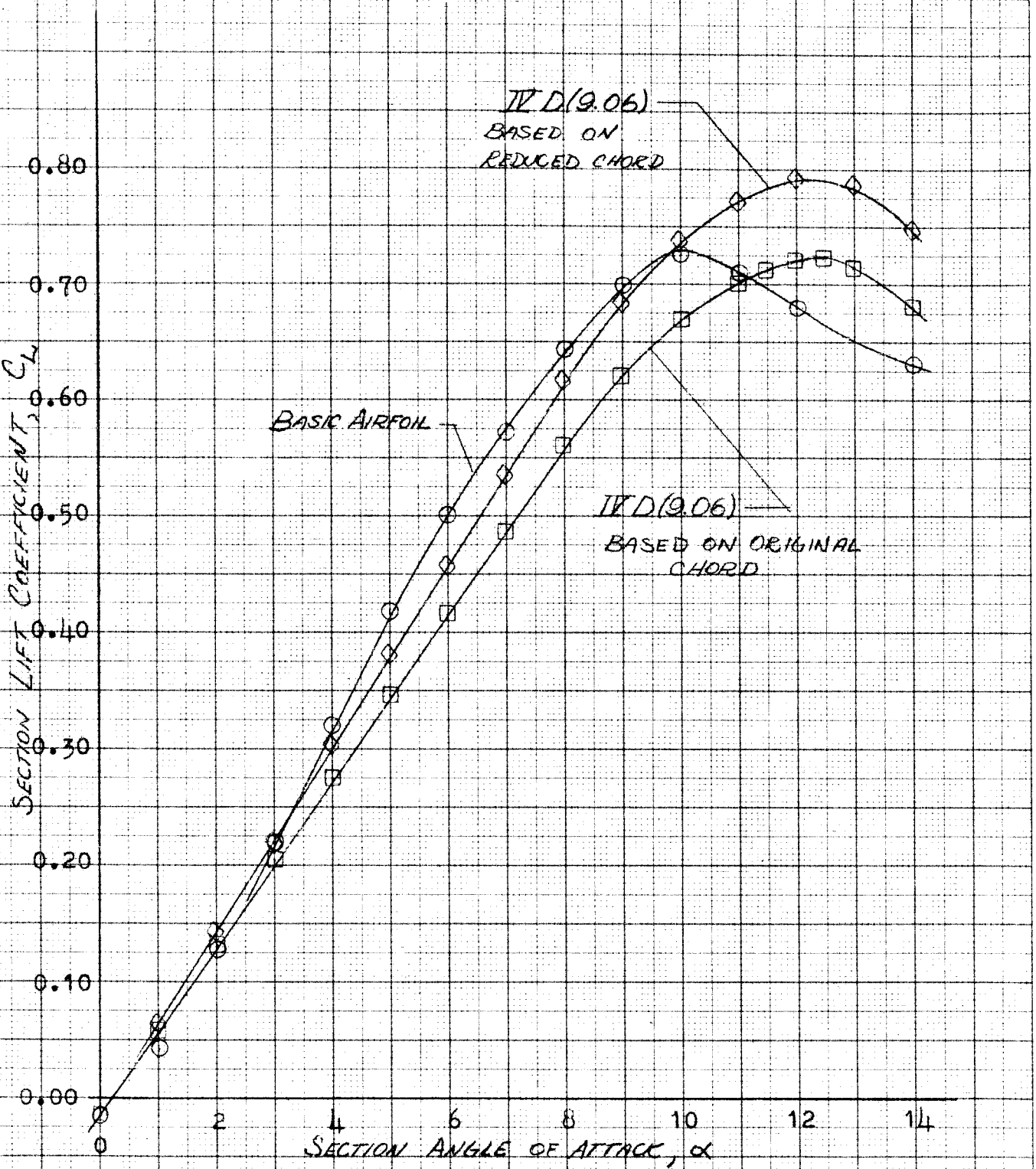

FIG. 17 - DIFFERENCE IN LIFT CURVES USING ORIGINAL AND REDUCED CHORD.

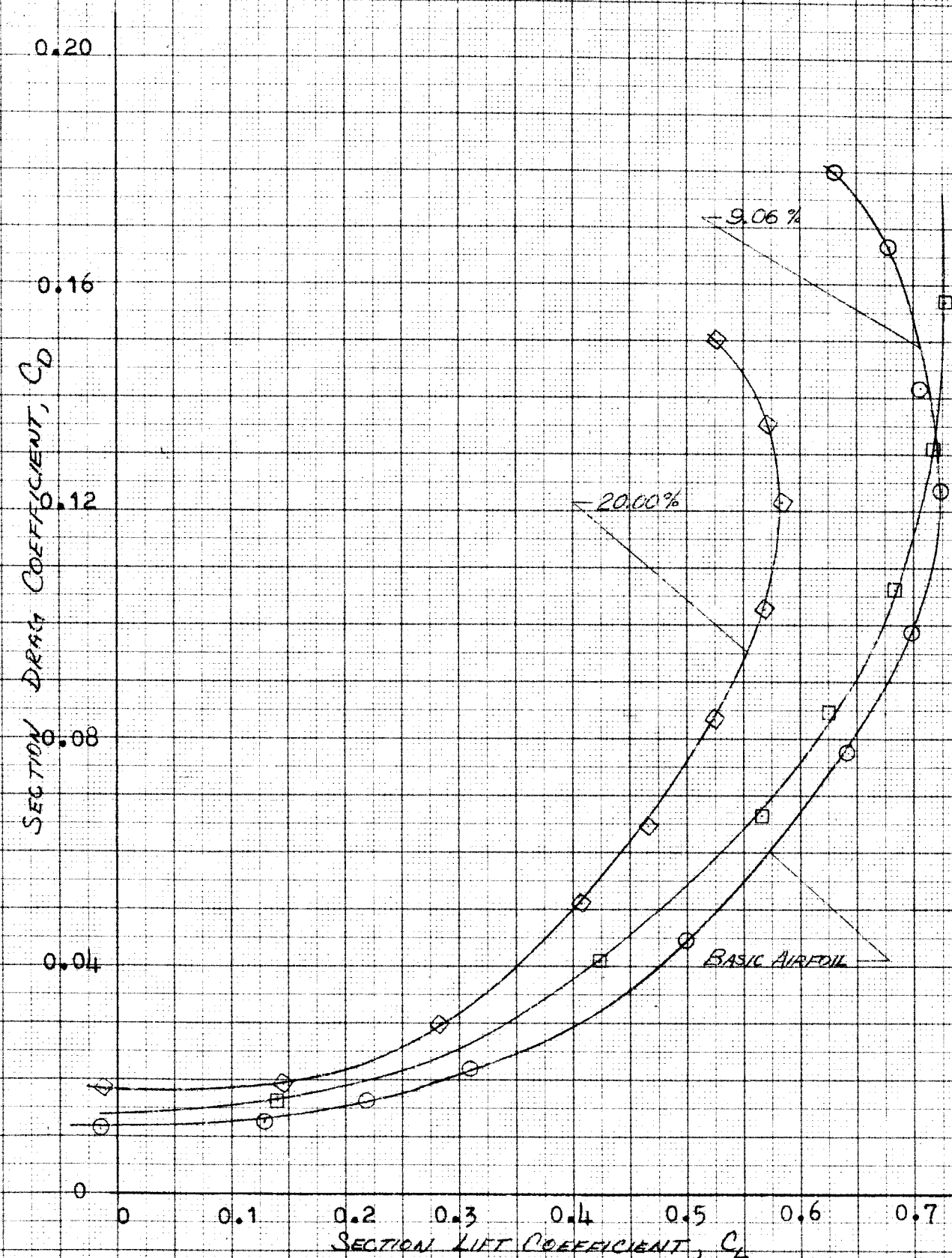

FIG. 18 DRAG POLARS, CONFIGURATION II A

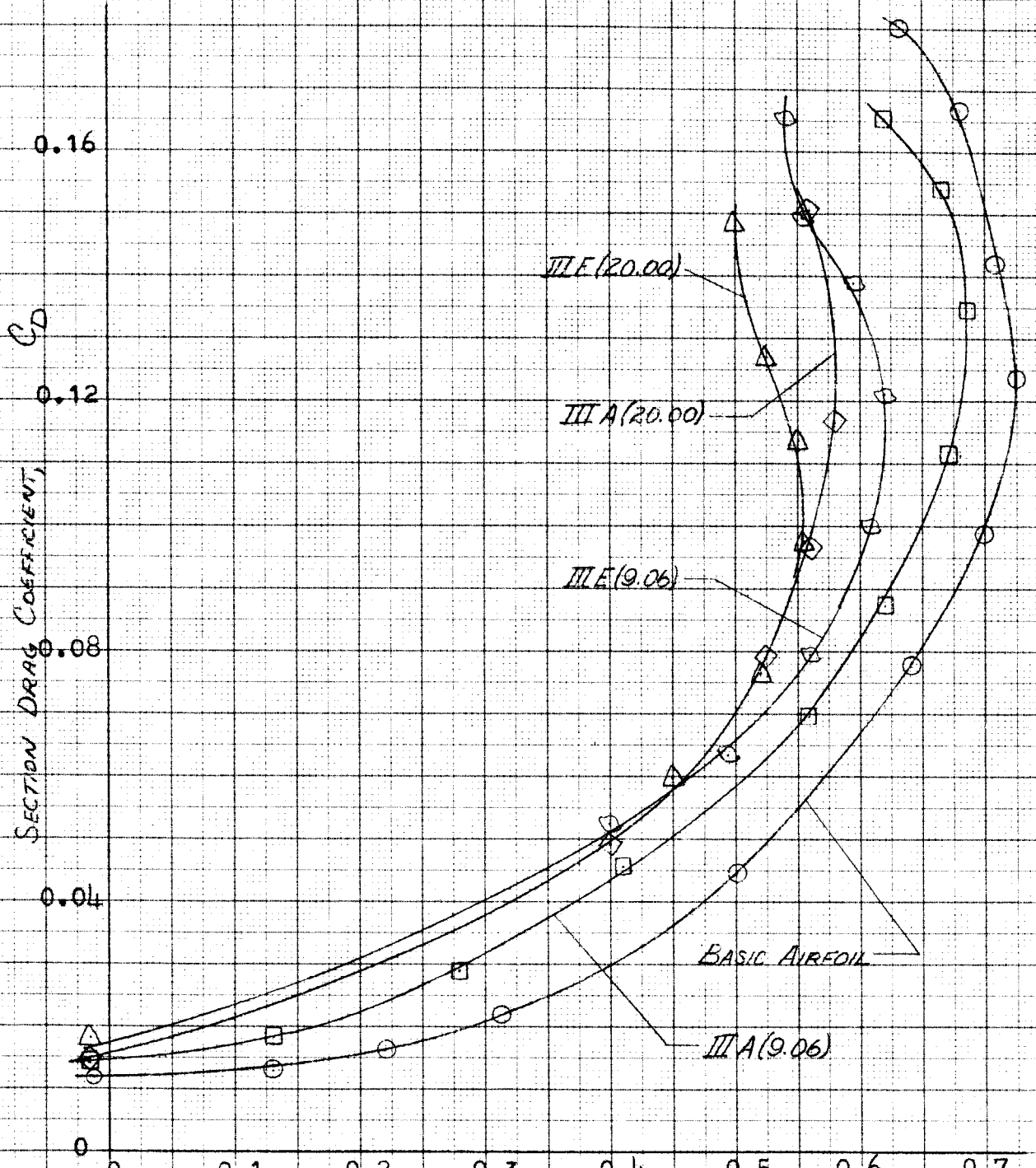

FIG. 19 - DRAG POLARS, CONFIGURATION IIIA.

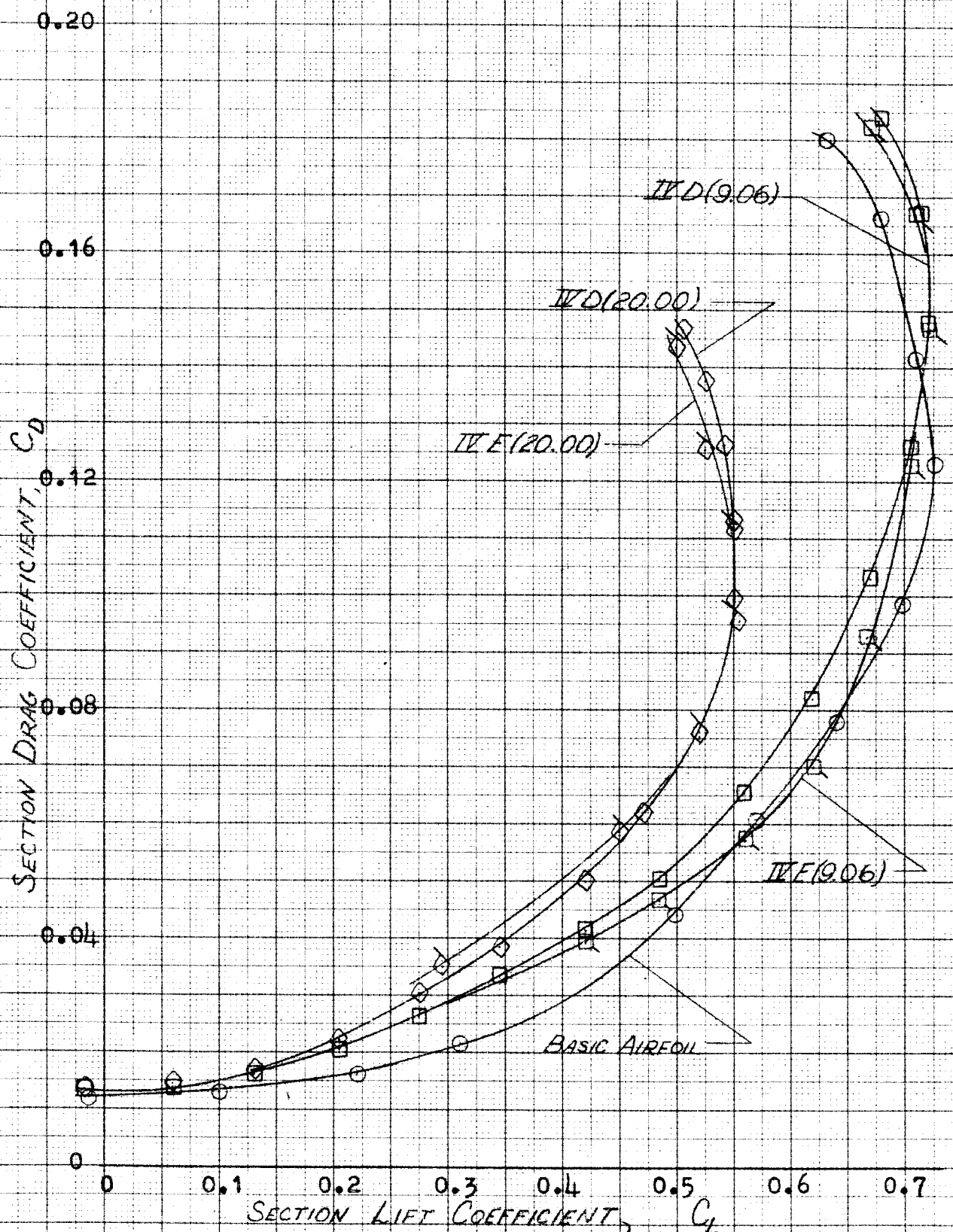

FIG. 20 - DRAG POLARS, CONFIGURATION IV.

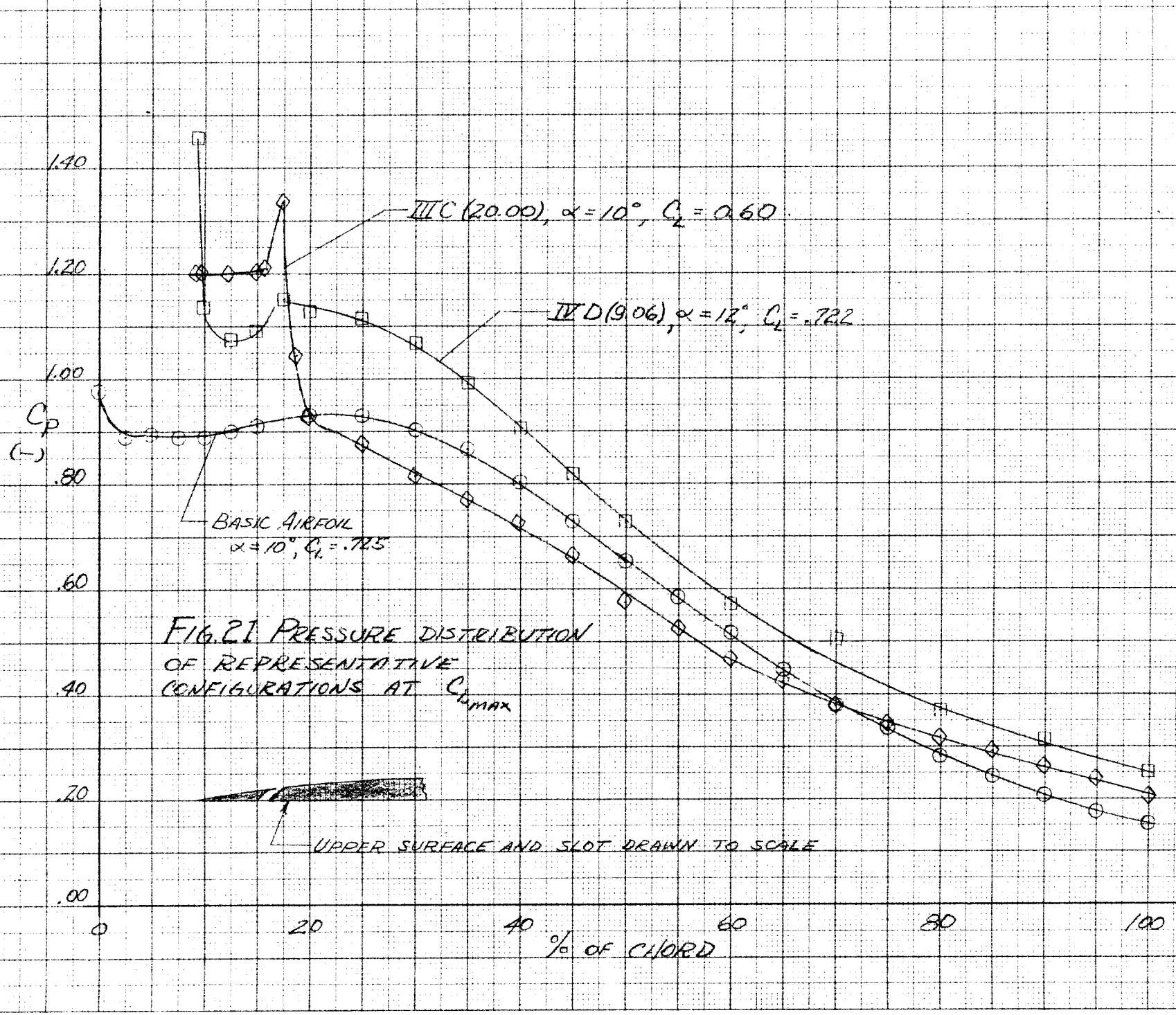

FIG. 21 PRESSURE DISTRIBUTION OF REPRESENTATIVE CONFIGURATIONS AT $C_{L_{MAX}}$

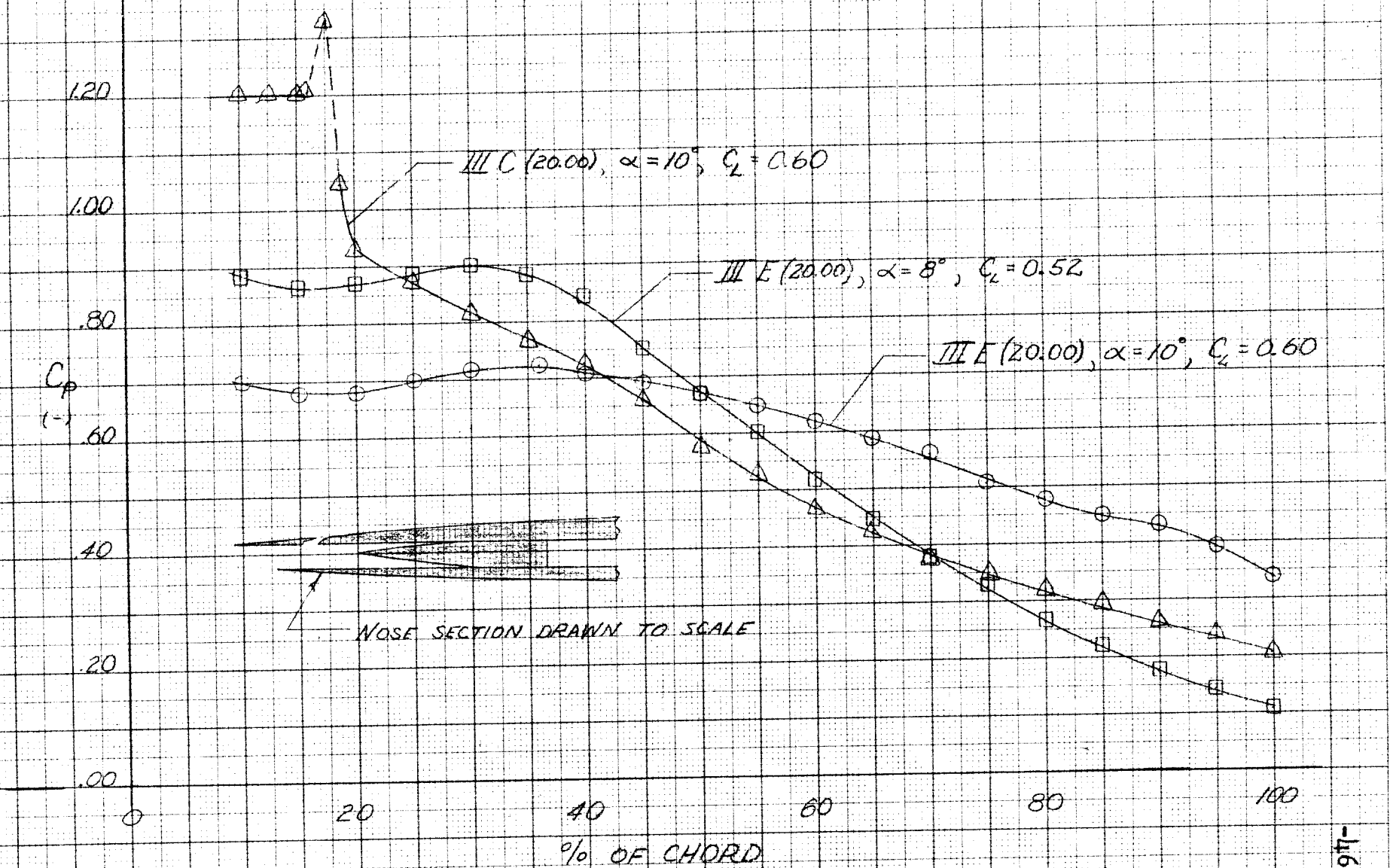

FIG. 22. EFFECT OF SLOT ON PRESSURE DISTRIBUTION, UPPER SURFACE

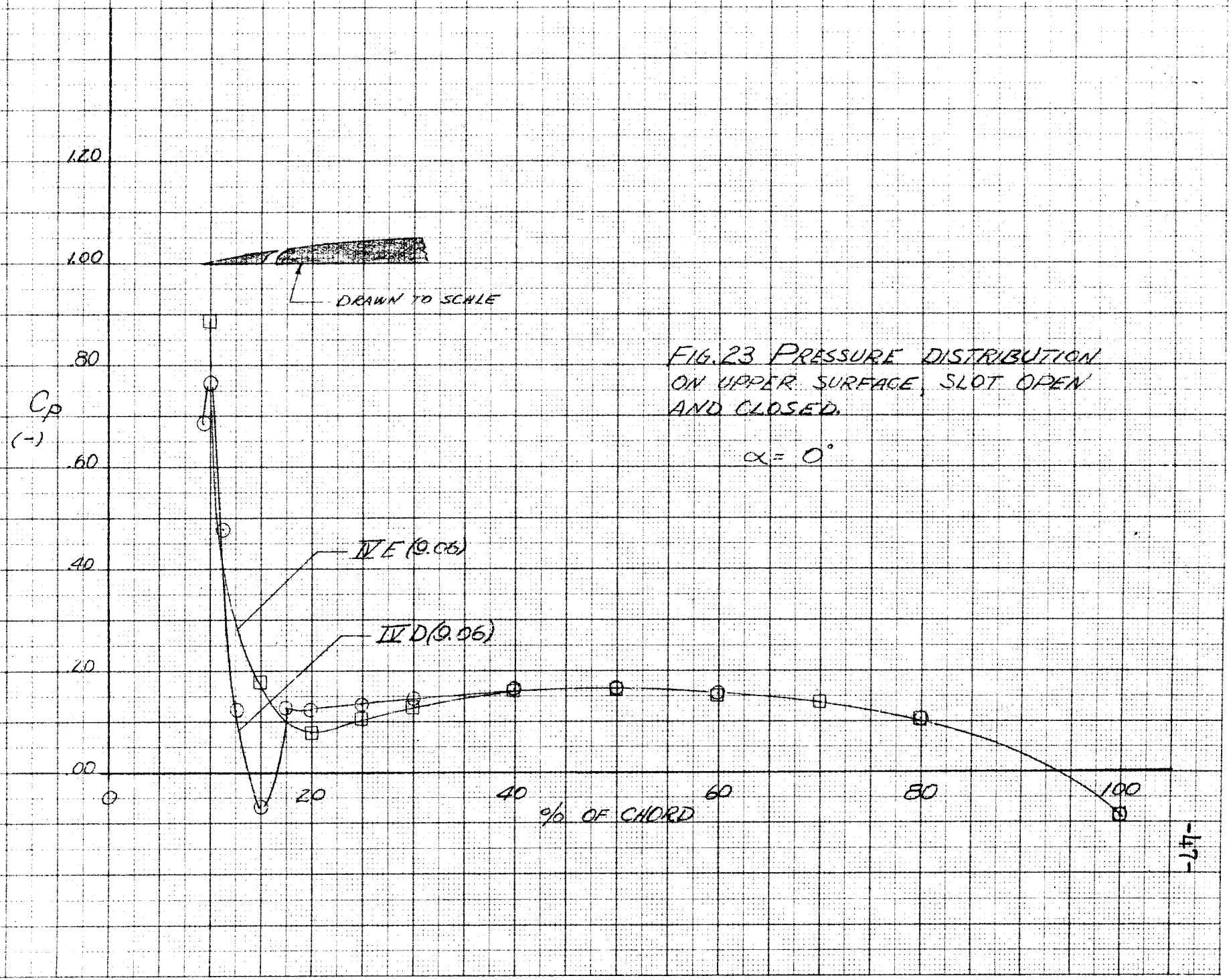

FIG. 23 PRESSURE DISTRIBUTION ON UPPER SURFACE, SLOT OPEN AND CLOSED.

$\alpha = 0°$

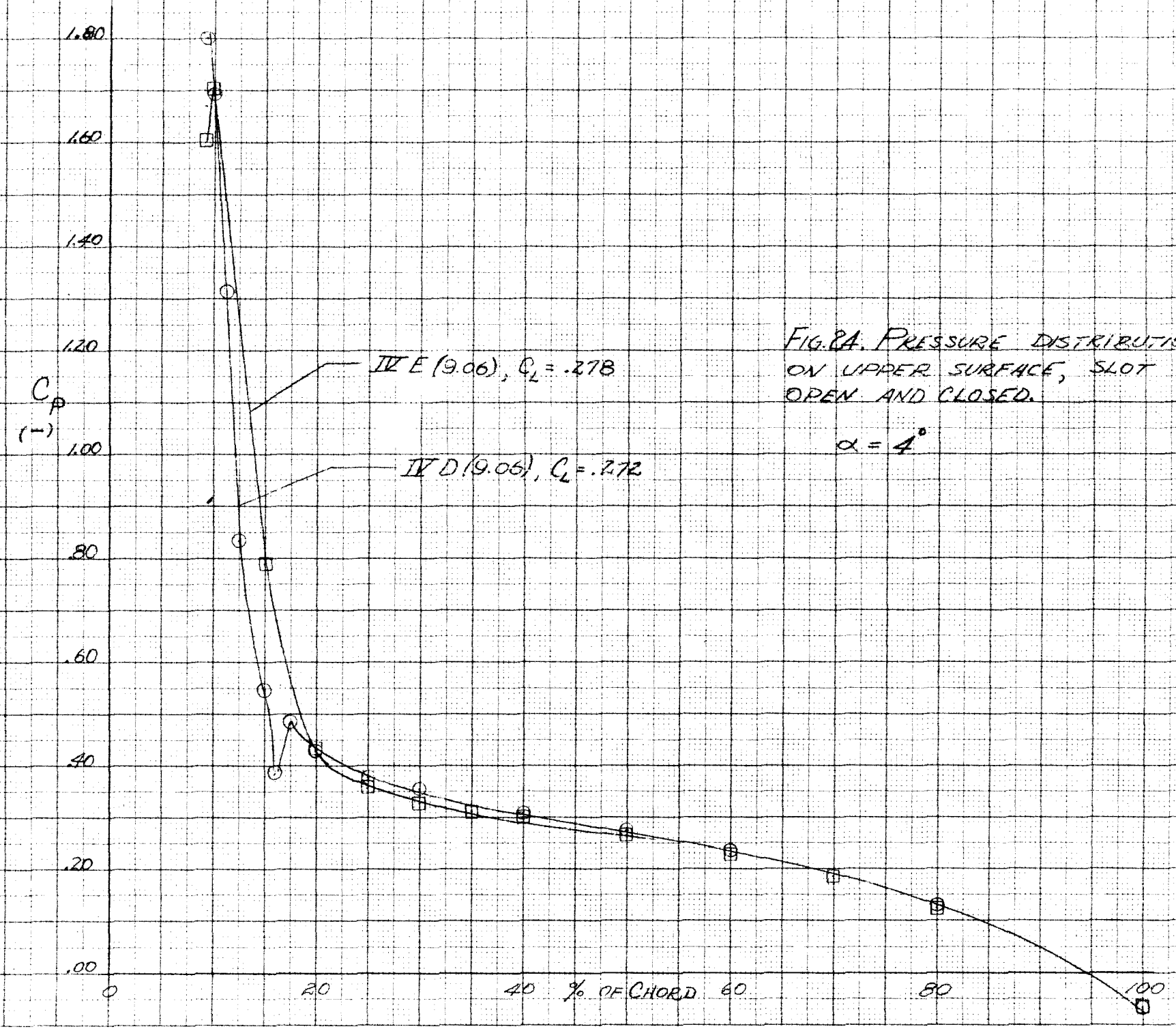

FIG. 8A. PRESSURE DISTRIBUTION ON UPPER SURFACE, SLOT OPEN AND CLOSED.

$\alpha = 4°$

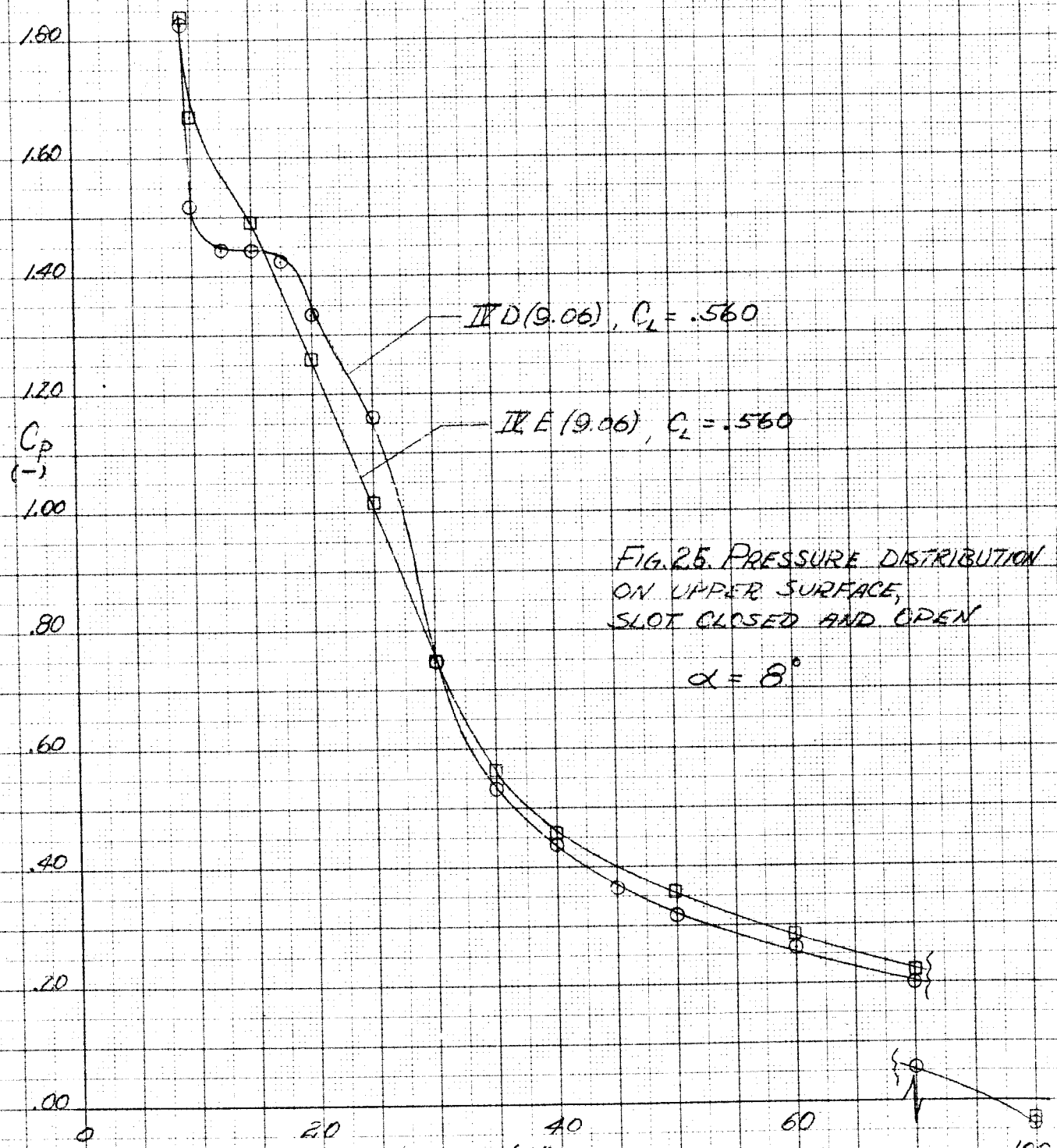

FIG. 25 PRESSURE DISTRIBUTION ON UPPER SURFACE, SLOT CLOSED AND OPEN

$\alpha = 8°$

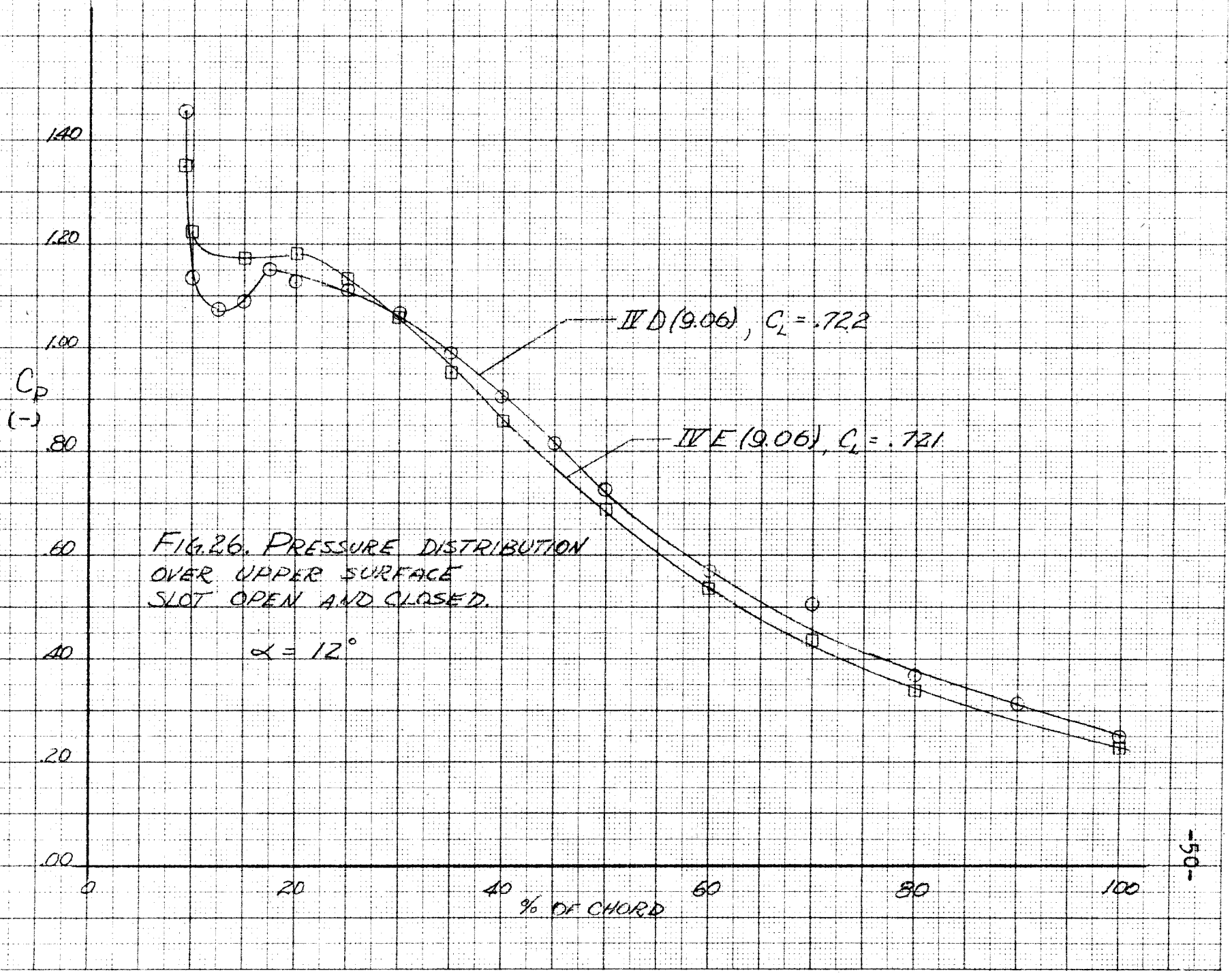

FIG. 26. PRESSURE DISTRIBUTION OVER UPPER SURFACE SLOT OPEN AND CLOSED.

$\alpha = 12°$